ISTANBUL TECHNICAL UNIVERSITY ★ GRADUATE SCHOOL OF SCIENCE ENGINEERING AND TECHNOLOGY

INVESTIGATION OF THERMAL AND MECHANICAL BEHAVIOR OF CARBON NANOTUBE REINFORCED ULTRA-HIGH MOLECULAR WEIGHT POLYETHYLENE COMPOSITES UNDER CRYOGENIC CONDITIONS

M.Sc. THESIS

Gülşah BAHÇELİ

Department of Aeronautics and Astronautics Engineering

Aeronautics and Astronautics Engineering Programme

JUNE 2019

ISTANBUL TECHNICAL UNIVERSITY ★ GRADUATE SCHOOL OF SCIENCE ENGINEERING AND TECHNOLOGY

INVESTIGATION OF THERMAL AND MECHANICAL BEHAVIOR OF CARBON NANOTUBE REINFORCED ULTRA-HIGH MOLECULAR WEIGHT POLYETHYLENE COMPOSITES UNDER CRYOGENIC CONDITIONS

M.Sc. THESIS

Gülşah BAHÇELİ

(511171111)

Department of Aeronautics and Astronautics Engineering

Aeronautics and Astronautics Engineering Programme

Thesis Advisor: Assoc. Prof. Hülya CEBECİ

JUNE 2019

İSTANBUL TEKNİK ÜNİVERSİTESİ ★ FEN BİLİMLERİ ENSTİTÜSÜ

KARBON NANOTÜP TAKVİYELİ ULTRA YÜKSEK MOLEKÜL AĞIRLIKLI POLİETİLEN KOMPOZİTLERİN TERMAL VE MEKANİK DAVRANIŞLARININ KRİYOJENİK KOŞULLAR ALTINDA İNCELENMESİ

YÜKSEK LİSANS TEZİ

Gülşah BAHÇELİ
511171111

Uçak ve Uzay Mühendisliği Anabilim Dalı

Uçak ve Uzay Mühendisliği Programı

Tez Danışmanı: Doç. Dr. Hülya CEBECİ

HAZİRAN 2019

Gülşah BAHÇELİ, a MSc. student of ITU Graduate school of Science Engineering and Technology student ID 511171111, successfully defended the thesis entitled "INVESTIGATION OF THERMAL AND MECHANICAL BEHAVIOR OF CARBON NANOTUBE REINFORCED ULTRA-HIGH MOLECULAR WEIGHT POLYETHYLENE COMPOSITES UNDER CRYOGENIC CONDITIONS", which she prepared after fulfilling the requirements specified in the associated legislations, before the jury whose signatures are below.

Thesis Advisor:	**Assoc. Prof. Hülya CEBECİ** Istanbul Technical University	.....
Jury Members:	**Prof. Vedat Ziya DOĞAN** Istanbul Technical University	.....
	Asst. Prof. Özgür DEMİR Yildiz Technical University	.....

Date of Submission : 03.05.2019
Date of Defence : 12.06.2019

To my family,

FOREWORD

First, I am grateful to my advisor Assoc. Prof. Hülya Cebeci for her guidance, contributions and her helps in every aspect especially on enriching my research vision since I was an undergraduate student. Also, I would like to thank to Dr. Bilim Atli-Veltin for her valuable insights and advices, which have steered my future career.

I am also grateful to Boeing Company for scholarship support during my master science study and ITU-AYP-2017-6 project for providing material support.

During laboratory studies in the Netherlands, I am thankful to TNO Structural Dynamics Laboratory members. Also special thanks to Ramon van Rooij and Dennis Wilbers for their manufacturing helps and Ramona Arts for SEM imaging at Teijin Aramid. Furthermore, I would like to thank to Dr. Binnur Aydoğan, Erhan Demirel, and Deniz Köken for their characterization supports. I would like to give my special thanks to my friends and colleagues in Nanomaterials, Textiles and Advanced Composites Research Group in Aerospace Research Center, in Istanbul Technical University. I am especially grateful to Dr. İpek Ösken for her recommendations during writing the thesis, İdris Gürkan for his helps during composite processing also Çiğdem Çağlayan and Beyza Bozali for their supports and helps in every time.

I would like to thank to my family; my mother Nesrin Bahçeli, my father Osman Bahçeli, and my brother Mithat Bahçeli for their supporting me all the time. Last, I am especially thankful to Coşkun Uluçeşme for his encouragement and belief in me.

June 2019

Gülşah BAHÇELİ

(Aeronautical Engineer)

TABLE OF CONTENTS

Page

ABBREVIATIONS

HDPE	: High Density Polyethylene
UHMWPE	: Ultra-high Molecular Weight Polyethylene
PE	: Polyethylene
CTE	: Coefficient of Thermal Expansion
SPC	: Single Polymer Composite
PC	: Polycarbonate
CNT	: Carbon Nanotube
PNC	: Polymer Nanocomposite
GO	: Graphene Oxide
PVA	: Polyvinyl Alcohol
PHAE	: Polyhydroxyaminoether
PCL	: Polycaprolactone
PA12	: Poly(dodecano-12-lactam)
PBT	: Polybutylene terephthalate
LDPE	: Low Density Polyethylene
TEM	: Transmission Electron Microscopy
XRD	: X-Ray Diffraction
SiC	: Silicon Carbide
VE	: Vinyl Ester
BP	: Buckypaper
ILSS	: Interlaminar Shear Strength
TPU	: thermoplastic Polyurethane
EMI	: Electro Magnetic Interference
PMI	: Polymethacrylimide
DMF	: Dimethylformamide
PTFE	: Politetrafloroetilen
SBS	: Short Beam Shear
BET	: Brunauer, Emmett and Teller
LNG	: Liquid Natural Gas
LOX	: Liquid Oxygen
LH_2	: Liquid Hydrogen
LN_2	: Liquid Nitrogen
PET	: Polyethylene terephthalate
PES	: Poly (ether sulphone)
PA	: Polyamide
PP	: Polypropylene
GF	: Glass Fiber
CF	: Carbon Fiber
CFRP	: Carbon Fiber Reinforced Polymer
PEI	: Polyetheylenimine
PEEK	: Poly (ether ether ketone)
ABS	: Acrylonitrile Butadiene Styrene

CVD	: Chemical Vapor Deposition
SWCNT	: Single Wall Carbon Nanotube
MWCNT	: Multi Wall Carbon Nanotube
SEM	: Scanning Electron Microscopy
TGA	: Thermal Gravimetric Analysis
ENF	: End Notch Flexure
DCB	: Double Cantilever Beam

LIST OF TABLES

Page

LIST OF FIGURES

Page

INVESTIGATION OF THERMAL AND MECHANICAL BEHAVIOR OF CARBON NANOTUBE REINFORCED ULTRA-HIGH MOLECULAR WEIGHT POLYETHYLENE COMPOSITES UNDER CRYOGENIC CONDITIONS

SUMMARY

Metal alloys have dominated materials specifically in aerospace and transportation industry for cryogenic applications; however, the growing demand on weight reduction impels researchers to progressively replace metallic materials with polymer matrix composites (PMCs). Exposing to cryogenic temperatures such as 77 K for liquefied natural gas (LNG), 20 K for liquid hydrogen (LH_2), and 2 K for liquid oxygen (LOX), causes a change in materials physical properties; therefore, selection criteria to operate in these temperatures are highly demanding to achieve thermal stability.

According to reported studies, thermoset polymers become brittle when experienced such low temperatures, which trigger the formation of cracks and delamination, thereby causes catastrophic failures of structure. To preclude such a brittle behavior of thermosets, thermoplastics are promising materials within their exceptional chemical resistance, ease of manufacture, thermal stability and recyclability as an environmentally friendly alternative material to nonrecyclable thermosets.

The utilization of ultra-high molecular weight polyethylene (UHMWPE) owing to exceptional properties as high tensile strength, low density, protecting its strength even at low temperatures and high chemical resistivity has been studied in the thesis. On the contrary to other materials, UHMWPE films tend to protect the load carrying capability and become stronger at very low temperatures than room temperature as desired for cryogenic applications. Despite the excellent mechanical performance of UHMWPE films under tensile loading, low shear strength and modulus between UHMWPE plies have been reported.

Reinforcing strategies including matrix toughening and interface toughening are mostly preferred to enhance interlaminar properties of laminated composites. The main drawback of matrix toughening is limited dispersion of reinforcing fillers into the matrix. Among the interface toughening strategies, the most common route is integrating nanomaterials to the structure without causing any weight penalty with efficient dispersion and distribution. Carbon nanotubes (CNTs) in a cylindrical form consisting of hexagonal lattice structure of carbons are widely used as reinforcing fillers. The intrinsic properties of CNTs resulting from high aspect ratio, chirality, and wall number are the predominant reasons of integrating CNTs to enhance performance of thermoplastics for wide range applications. For interface toughening, CNTs can be implemented through different methods such as directly growth of CNTs on fiber surface and interleaving paper-formed CNTs into the composite

interface. Growth of CNTs on substrate requires expensive equipment and relatively long production time. Hence, herein, interface toughening by interleaving paper-formed CNTs buckypapers (CNT BPs) has been studied, and will be named as CNT BP. The main motivation is to benefit from outstanding properties of CNTs such high strength-to-weight ratio, lightweight, foldability and being fabricated by relatively easier manufacturing process which is crucial to implement for industrial applications. The CNT interleaving technique also promotes increased life-time of composite by delaying formation and propagation of cracks and hindering delamination.

In the experimental part, first, fabrication of CNT BPs as interleaves is described in detail. The first interlayer which is CNT BP is fabricated by dispersing multi-walled CNTs in ethanol then filtered under vacuum. The effect of CNT interface thickness on the mechanical properties of composite, particularly interlaminar shear strength (ILSS) is investigated. The variation on the CNT layer thickness is obtained by fabricating CNT BPs in different weight percentages which are 0.05, 0.065, 0.13 and 0.2. As an alternative to CNT BPs, the second type of CNT interlayer is fabricated by melt mixing method to achieve homogenously dispersed CNTs within the polymer. High density polyethylene (HDPE) granules are mixed with CNTs through twin-screw extruder at elevated temperature, then CNT/HDPE granules are heated and pressed to form thin film CNT/HDPE core layer.

In the second chapter, the CNT core layer reinforced UHMWPE laminated composite fabrication details are described. CNT BP and CNT/HDPE films are placed at the mid-plane of UHMWPE films and composites are manufactured by hot press. Laminated composites are cut by water jet in certain dimensions as specified in the related mechanical test standard.

Thermal and morphological characterizations of CNT core layers and composites, also mechanical tests of composites are assessed. Mechanical tests are performed according to ASTM 2344D standard to measure the interlaminar shear strength (ILSS) of composites at room and cryogenic environment which is LN_2 temperature (77 K). Thermal characterizations of CNT films are performed by thermogravimetric analysis (TGA) and differential scanning calorimetry (DSC) to correlate relationship between mechanical performance of composites and the change in crystalline structure after exposed to cryogenic temperature and to evaluate impregnation quality of CNT BPs. The morphologic analyses which are scanning electron microscopy (SEM), optical microscopy and Brunauer, Emmett and Teller (BET) surface analysis reveal the impregnation qualities of CNT BPs. Specific surface area and porosity are calculated from BET results and the results are evaluated in conjunction with TGA results.

The ILSS of UHMWPE composite is enhanced by the insertion of 0.05 wt% CNT BP by 9.5%, 0.065 wt% CNT BP by 6.4%, and melt mixed CNT/HDPE film by 13% at room temperature. At cryogenic temperature, ILSS is increased by 3.2% after CNT/HDPE film interleaving.

KARBON NANOTÜP TAKVİYELİ ULTRA YÜKSEK MOLEKÜL AĞIRLIKLI POLİETİLEN KOMPOZİTLERİN TERMAL VE MEKANİK DAVRANIŞLARININ KRİYOJENİK KOŞULLAR ALTINDA İNCELENMESİ

ÖZET

Havacılık ve taşıma endüstrisinde kriyojenik uygulamalarda metal malzemelerin kullanımı ön plana çıkmaktadır. Ancak, yapının ağırlığının azaltılması için metal malzemelerin polimer esaslı kompozitlerle değişimi giderek artmaktadır. Kriyojenik sıcaklıklara maruz kalmak; ki bu sıcaklıklar sıvı doğal gaz (LNG) için 77 K, sıvılaştırılmış hidrojen (LH_2) için 20 K ve sıvılaştırılmış oksijen (LOX) için 2 K dir; malzemelerin fiziksel özelliklerinde değişikliğe yol açar. Bu sebepten dolayı, son derece düşük bu sıcaklıklara maruz kalan malzemelerin termal stabilitelerini korumaları gerekmektedir.

Havacılık ve uzay şirketleri tarafından yayımlanan raporlarda belirtildiği üzere termoset reçineler kriyojenik sıcaklıklara maruz kaldıklarında son derece gevrek davranış göstermeye başlarlar ve bu da çatlak oluşumunu ve ilerlemesini tetikleyerek malzenin hasara uğramasına sebep olur. Termoset polimerlerin çapraz bağlı yapısından kaynaklı bu olumsuz etkinin engellenmesi için kimyasal direnci ve termal stabilitesi yüksek, yüksek darbe dayanımlı, kolay üretilebilen ve geri dönüştürülebilen termoplastik polimerlerin kullanılması alternatif bir çözüm yolu olarak öne çıkmaktadır.

Termoplastik polimerler arasında ise ultra yüksek molekül ağırlıklı polietilen (UHMWPE) filmin sahip olduğu yüksek çekme dayanımı, düşük yoğunluk, düşük sıcaklıklarda dayanımını koruması bu çalışmada kullanılmasının başlıca nedenleri arasındadır. Yapılan çalışmalarda ise UHMWPE'nin kriyojenik sıcaklıklarda termoset polimerlerin aksine dayanımında artış olduğu ve sünek yapılarını koruyabildikleri gözlemlenmiştir. Ancak, çekme dayanımının aksine katmanlar arası kesme mukavemetinin son derece düşük olduğu da ispatlanmıştır.

Kompozit malzemeleri iyileştirme yöntemleri reçine iyileştirmesi ve ara yüzey iyileştirmesi olarak iki ana başlık altında özetlenebilir. Matris dayanımını arttırma yönteminde katkı malzemesinin homojen şekilde dağıtılamaması malzemenin özelliklerini olumsuz yönde etkiler. Ara yüzey iyileştirmesinde ise nanomalzeme kullanmak kütle artışı olmadan güçlendirme sağlamak için çok sık tercih edilen yöntemlerdendir. KNT'ler altıgen şeklinde bağlanmış karbon atomlarının tek bir grafen tabakası meydana getirdikten sonra silindirik şekil almalarıyla oluşur ve yaygın olarak kullanılırlar. Sahip oldukları yüksek açıklık oranı, kiraliteleri ve duvar sayıları KNT'lerin üstün mekanik, elektriksel ve ısıl özellikler kazanmalarını ve birçok uygulamada kullanılmalarını sağlar. Ara yüzey iyileştirmesi için kullanılmalarında farklı yöntemler izlenebilir bunların başlıcaları ise fiber üzerinde büyütmek ve kağıt formunda üretip polimer katmanları arasına yerleştirmektir. Fiber üzerinde KNT büyütmek ekipman ve prosedür açısından maliyeti yüksek bir yöntem

olduğu için, bu çalışmada kağıt formundaki KNT ara yüzeylerinden yararlanılmıştır. Kâğıt formundaki KNT'ler literatürde 'buckypaper'(BP) olarak adlandırılmaktadırlar ve sahip oldukları yüksek mukavemet, düşük ağırlık özellikleri ve nispeten kolay üretim yöntemleriyle hızlı endüstriyel uygulamalar için son derece uygundurlar. Ara yüzey iyileştirme yöntemleriyle kompozitte çatlak oluşumu geciktirilir, çatlak ilerlemesi ve tabaka ayrılması engellenir nihai olarak da yapının ömrü uzatılır.

Tezin deneysel kısmında ilk olarak KNT ara yüzeylerinin üretimleri detaylı şekilde açıklanmıştır. Ara yüzey olarak kullanılacak olan KNT BP çok duvarlı KNT'lerin ses üstü dalga üreten sonikatör kullanarak etanolde dağıtılmasıyla ve sonrasında vakum filtrasyon sistemi yardımı ile filter kağıdı üzerinde biriktirilerek BP formu alması sağlanmıştır. Sonrasında elde edilen KNT BP'ları filter kağıdından ayrıştırılıp, fırında kurutularak etanolün uçurulması sağlanmıştır. Böylece sadece KNT içeren kağıt formunda bir ara yüzey elde edilmiştir. Kullanılan ara yüzeyin kalınlık değişiminin, kompozitin ara yüzey kesme dayanımı üzerindeki etkisi farklı ağırlık yüzdelerinde KNT kullanılarak farklı kalınlıklara sahip BP'lar üretilerek incelenmesi amaçlanmıştır. Bu ağırlık yüzdeleri ise 0.05, 0.065, 0.13 ve 0.2'dir. Aynı zamanda, KNT BP'a alternatif olarak ikinci bir tip KNT ara yüzeyi eriyik karıştırma yöntemiyle üretilmiştir. Endüstriyel uygulamalar için hızlı bir üretim yolu olan bu yöntem ile KNT'lerin homojen dağıtımı daha kolay ve etkili bir şekilde gerçekleştirilmektedir. Bu yöntemin çalışmaya dahil edilmesiyle birlikte kimyasal işlemler gerektiren BP üretimiyle kıyaslanması hedeflenmiştir. KNT film ara yüzeyi, yüksek yoğunluklu polietilenin (HDPE), çift vidalı ekstrüderde eritilip KNT ile karıştırılmasıyla ve elde edilen KNT/HDPE taneciklerinin sıcak preste basılarak ince film formu alması sağlanarak üretilmiştir.

Tezin ikinci bölümünün ise KNT ara yüzeyi entegre edilmiş kompozitlerin üretimi açıklanmıştır. Bu kapsamda, oluşan KNT BP ve KNT/HDPE filmleri, UHMWPE filmlerinin orta katmanına yerleştirilmiş olup, UHMWPE filmi üreticisi tarafından belirlenen sıcaklık ve basınç altında basılmıştır. Mekanik test için standarda uygun boyutlardaki kompozitler su jeti kullanılarak kesilmiştir.

KNT ara yüzeylerine ve kompozitlere uygulanan ısıl ve morfolojik karakterizasyonlar ile gerçekleştirilen mekanik testler detaylı şekilde değerlendirilmişlerdir. Kompozitlerin ara yüzey kesme dayanım ölçümü ASTM 2344D testine göre oda sıcaklığı ve kriyojenik sıcaklıkta ki bu sıcaklık LH_2 sıcaklığıdır (77 K) gerçekleştirilmiştir. UHMWPE kompozitin ara yüzey kesme dayanımı oda sıcaklığında, , % 0.05 KNT ağırlık yüzdesindeki BP kullanılarak %9.5, % 0.065 KNT ağırlık yüzdesindeki BP ile % 6.4 ve KNT/HDPE film kullanılarak % 13 arttırılmıştır. Kriyojenik ortamda ise bu dayanım KNT/HDPE film entegrasyonu ile % 3.2 arttırılmıştır.

Kriyojenik sıcaklıklara maruz kalmanın, KNT/HDPE filmi kristal yapısı üzerindeki etkisi ve KNT BP'ların polimer ile emdirilme kalitesi taramalı elektron kalorimetresi (DSC) ve termogravimetrik analiz (TGA) ile araştırılmıştır. Bu analizler sonucu malzemelerin kristal yapısı ile mekanik dayanımı arasında ilişki kurulmuştur. Elde edilen sonuçlara göre polimer yapıya KNT eklemenin, çekirdeklenme alanları oluşturarak polimerin kristalinitede artışı sağladığı sonucuna varılmıştır. Bununla birlikte, kriyojenik sıcaklıklara maruz kalmanın kristalinite oranında azalmaya sebep olduğu anlaşılmıştır. Kriyojenik şartlarda gerçekleştirilen testlerde gözlemlenen ara yüzey dayanımının iyileştirilmesindeki azalışın sebebi de krtistalinitenin azalmasıyla bağdaştırılmıştır. Morfolojik analiz çalışmalarında ise taramalı elektron mikroskobu

(SEM) ve ışık mikroskobuyla BP'ların ıslaklığı ve UHMWPE film ile yapışma kalitesi kontrol edilmiştir. Böylece, en etkin yapışmanın KNT/HDPE film arayüzeyi kullanılarak elde edildiği saptanmıştır ve bu sonuçlar da yüksek mekanik dayanım sonuçlarıyla desteklenmiştir. Brunauer, Emmett ve Teller (BET) analizi ile ise BP yüzey alanı hesaplanmış olup, yapı içerisindeki gözenek oranı araştırılmıştır. BET analizinden elde edilen veriler ile TGA hesaplamaları doğrulanmış ve desteklenmiştir.

1. INTRODUCTION

1.1 Literature Review

1.1.1 Thermoplastic composites

Thermoset polymers are highly sought by means of high temperature, moisture resistance and high fracture toughness for advanced applications. However, limited shelf life and non-recyclability urge researchers to focus on benefiting from thermoplastics. Thermoplastics have long polymer chains associate by intermolecular forces and formed of chemically independent macromolecules without any crosslinks, which brings flexibility to the polymer with increased temperature [1]. Hence, permanent deformation does not occur through polymer chains during processing below degradation temperature, which allows reforming and recycling. According to the molecular structure, thermoplastics can be classified in two groups which are amorphous and semi-crystalline as illustrated in Figure 1.1. The term "crystalline" defines regular and compacted lattice structure of polymer chains and induces strength and rigidity to the polymer. By changing cooling rate during processing, the amount of crystalline in structure varies; therefore, melting temperature of material is changed and specified. Amorphous part in a polymer allows the remolding capability through random bundles as a prominent feature of thermoplastics [2].

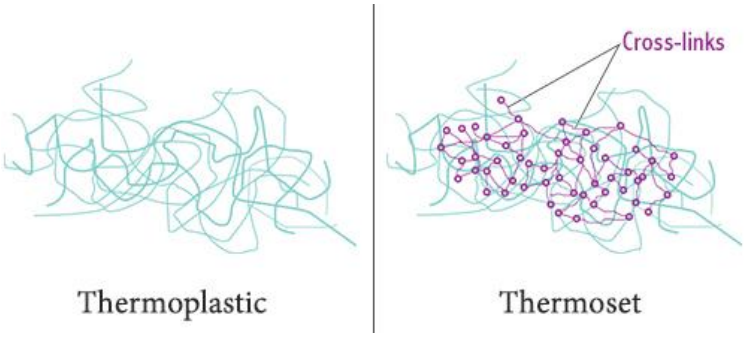

Figure 1.1: Chemical structure of thermosets and thermoplastics [2].

The essential chemical difference between thermosets and thermoplastics is viscosity behavior with increasing temperature as presented in Figure 1.2. At low

temperatures, both thermosets and thermoplastics act like a solid. However, thermoset polymers show parabolic viscosity curve with increasing temperature, which defines the easy movement of chains at low temperatures. After the irreversible hardening reaction, during chemical cross-linking, chain movement is hindered and viscosity dramatically increases at specific temperature. On the contrary to thermosets, the viscosity of thermoplastics continuously decreases and polymers become malleable with increasing temperature. This striking difference in viscosity behavior results in recyclability and reforming capability of thermoplastics [3]. Literature studies show that thermoplastics are also potential candidates to be used in the structural parts within their intrinsic properties [4]. Likewise, high strength-to-weight ratio and chemical resistance of thermoplastics have profound effect on making these materials considerable candidates in aircraft components [5, 6].

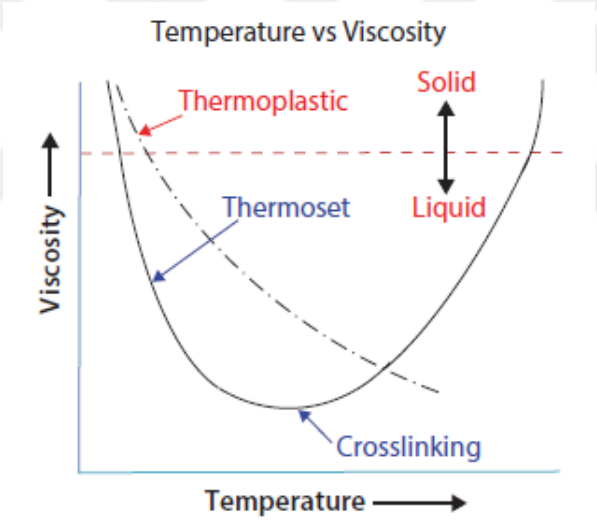

Figure 1.2: Viscosity behaviors of thermosets and thermoplastics with respect to increasing temperature [3].

The major processing techniques employed for thermoplastics are molding, extrusion, thermoforming and automated fiber placement *etc*. Thermoplastic molding is reversible processing technique where sheets and/or pellets are melted, then forced into mold for consolidation, cooled to harden and demolded. This technique has high output rate and cost-effective processes, which results in time-efficient manufacturing standard for industry.

As mostly preferred approach, compression molding method is used to mold thermoplastic laminated composites into the desired shape with a combination of

pressure and temperature by stacking polymer films, fiber prepregs, or metallic/ceramic microstructures. Thermoplastic composites generally consist of fiber, nanomaterials or micro/nano-particle reinforced structures. Mechanical performance of the desired architecture is arranged by changing the orientation and amount of fiber/film/nanomaterials also number of plies.

With the growing interest in thermoplastic, in a wide material field expanding from high performance thermoplastics to mass products, performance evaluation of thermoplastics has been accelerated. Lin *et al.* [7] combined dissimilar thermoplastics which are polypropylene (PP) and polyethylene terephthalate (PET) to enhance the multi-properties of neat PP laminated composite. The achieved impact and tensile strength increments were 320 % and 44 %, respectively by integrating PET fabric. Inclusion of nanomaterials and carbon or glass fibers to the composite is an alternative reinforcing strategy for thermoplastics to tailor mechanical and/or thermal characteristics of polymers. For high-performance thermoplastics, polyetheretherketone (PEEK) prepregs with carbon fiber plies and magnesium sheets were subjected to tensile loading. Consequently, PEEK prepregs with carbon fiber plies exhibited higher tensile strength than neat magnesium sheets by taking advantage of high strength of carbon fiber and PEEK prepregs [8].

1.1.2 Thermoplastic composites and their potential use in cryogenic applications

Recently, cryogenic substances get an increasing interest by researchers to be used as a fuel instead of fossil fuels for clean energy sources. Liquefied natural gas (LNG) is the most well-known cryogenic substance owing to its wide usage area as a fuel in industry and daily life. In space applications, liquid oxygen (LOX) and liquid hydrogen (LH_2) are innovatively used for combustion and clean energy source for rockets as a propellant combination over the past years. Cryogenic substances are liquefied to keep in liquid state below their boiling temperatures for volume reduction. Eventually, storage and transportation of these substances become more economical and easier. Up to date, even though metallic materials are highly deployed for cryogenic tanks, research on the development of composite cryogenic tanks has been accelerated as a cutting-edge technology in recent years for weight-saving solutions. The translation of weight reduction into cost saving in aerospace industry impels researchers to gradually replace metallic materials particularly,

aluminum alloys, lithium, and stainless steel, with polymer matrix composites (PMCs) in order to flourish the physical and mechanical properties of structural components. Beyond the structural parts, cryogenic tanks, where cryogenic substances including LNG, LH_2 or LOX are stored and transported, occupy huge area and weight specifically in aerospace structures. Structural materials hosting these substances expose to extremely low operational temperatures such as 77 K for LNG, 20 K for LH_2, and 2 K for LOX; therefore, materials should withstand and protect their thermal stability while working such low temperatures and high pressures. Composite structures are reliable and promising materials as an alternative to conventional metallic materials to acquire lighter weight, thus cost-efficient designs (Figure 1.3a). In the case of honeycomb sandwich structure concept, which was developed by Northrop Grumman (Figure 1.3d), inner and outer surfaces of the vessel are made from carbon fiber/epoxy honeycomb sandwich structure as same as Lockheed Martin concept (Figure 1.3c). However, the structure is distinctly designed from the Lockheed Martin structure, by using additional aluminum foil between carbon fiber laminates to avoid hydrogen leakage [9]. The air between these two vessels is vacuumed and honeycomb structure directly interacted with the isolated area, which led to the failure of the structure depending on the penetration of cryogenic substances. Furthermore, in fluted core tank concept is designed by Boeing (Figure 1.3b), honeycomb core in fluted form was integrated to the tank to stiffen the structure against to stresses in the normal axis [10]. In the last decade, besides achievement on a more durable and stiffer structural parts, weight saving is accomplished up to 42.8 % by replacing metallic base material with composite structures [9].

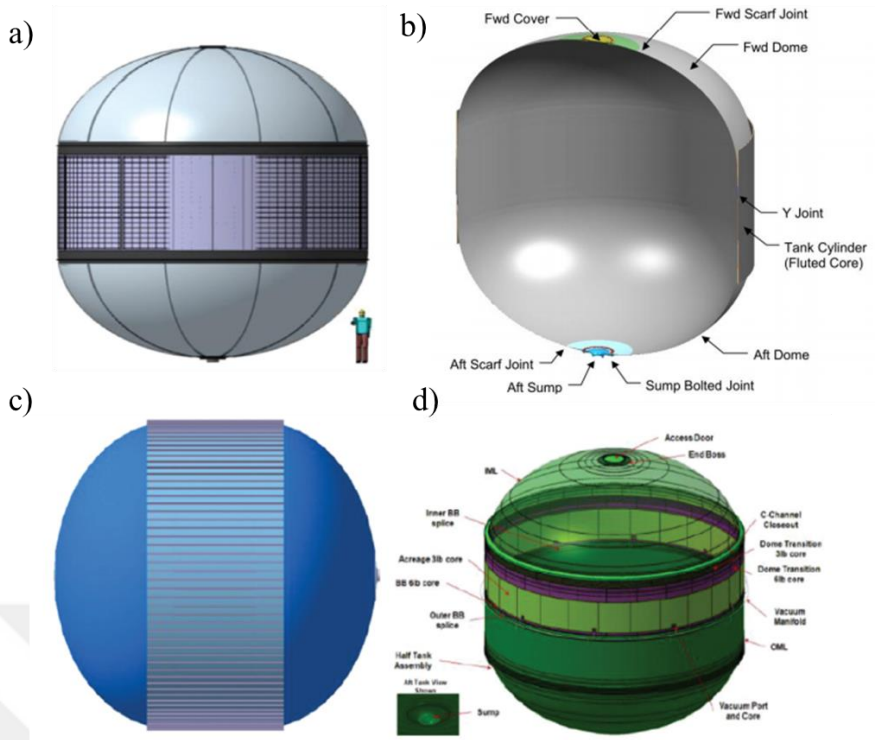

Figure 1.3: Different tank concepts; a) NASA Li-Al concept, b) Boeing fluted core concept, c) Lockheed Martin externally stiffened concept, d) Northrop Grumman honeycomb core sandwich composite concept [9].

Heretofore, significant effort is put into developing composite cryotanks made from carbon fiber reinforced thermoset composites. According to reported studies by NASA [11] and other aerospace companies like Lockheed-Martin or Northrop Grumman [9], thermoset polymers become brittle when experienced such low temperatures, which trigger the formation of cracks and delamination, thereby failure of the structure. To preclude such a brittle behavior of thermosets due to highly crosslinked microstructure, thermoplastics are promising materials within their exceptional chemical resistance, ease of manufacture and recyclability as an environmentally friendly alternative material over non-recyclable thermoset polymers.

Coefficient of thermal expansion (CTE) mismatch between fiber and matrix causes to microcrack formation while thermal cycling during operation which concludes with the leakage of cryogenic substances through the crack path. Accumulation of these microcracks can trigger catastrophic failures; a striking example for the failure is explosion of X-33 prototype. Hindering of formation and propagation of microcracks is still a challenging issue, thus many researchers are focused on the effects of thermomechanical loading on microcracking and failure of composites

under cryogenic conditions [12]. There is one promising solution named as single polymer composites (SPCs) to avoid CTE mismatching between matrix and reinforcement or to minimize it. This is based on using same polymer or polymers from same chemical family rather than fiber-matrix systems [13, 14].

Taking into consideration the superiorities of thermoplastic polymers over thermoset polymers, comprehensive studies revealed the mechanical performance alteration of thermoplastic composites at ultra-low temperatures. In the feasibility evaluation of thermoplastics for cryogenic applications, reliable composite tanks made from engineering thermoplastics such as polyethylene (PE) [15], PP [16], and polycarbonate (PC) [17] have been tested to prove their enhanced mechanical properties; tensile strength, toughness and Young's modulus; at cryogenic temperatures compared to their performances at room temperature. Considerable research efforts are devoted to enhance the weakness of thermoplastic composites by reinforcing with carbon nanotubes (CNTs). Wei *et al.* [17] studied on the investigation of flexural fatigue response and change in electrical resistance of polycarbonate (PC) strengthened with multi-wall carbon nanotubes (MWCNTs) at LN_2 temperature. Their investigation concluded that composites with CNT reinforcement showed higher fatigue resistance at cryogenic temperature in comparison with neat PC. In addition to PC, remarkable increase in mechanical performance, particularly impact strength, under cryogenic conditions was observed for PP composites fabricated with nanoclays by melt mixing method by Soleimani *et al.* [16].

Such low temperatures create substantial transition in mechanical characteristics of thermoplastics since chain mobility is restricted and chain flexibility is disposed of. The research conducted by Hongtao *et al.* [15] established that multi-mechanical properties of ultra-high molecular weight polyethylene (UHMWPE) alter when subjected to cryogenic temperatures. Hardness and wear resistance were clearly improved and compression strength of UHMWPE is almost 4-fold of its strength at room temperature. Based on this background, UHMWPE is particularly well suited material for low temperature applications because it is phenomenal load carrier even at cryogenic temperature besides its excellent chemical resistance.

1.1.3 Reinforcing strategies of thermoplastic composite materials

Overall performance of PMCs is altered with different reinforcing strategies such as fiber, particle, platelet *etc.* in micro, nano, or macro scale. Considering the weight limitations on structural parts in aerospace industry, nano scale reinforcements become prominent candidate for final material. Particularly in recent years, graphene is one of the remarkable reinforcing agents based on high thermal and electrical conductivity and flexibility, after subsequently extracted as a single carbon layer from graphite as shown in Figure 1.4a [18]. In cryogenic field, graphene and its oxidized form, graphene oxide (GO), have received attention to reinforce the fracture toughness [19] and interlaminar shear strength (ILSS) [20] (Figure 1.4b) of thermoset composites in several studies. Nonetheless, challenges in cost saving for fabrication processes and mass production with high quality restrict research and development activities on graphene. The other most well-known nanomaterial is silica nanoparticles consisting of silicon and oxygen atoms. Non-toxicity, dimensional stability, and availability for functionalization lead its usage as strengthening additive for divergent applications like medical, construction and microelectronics [21]. On the other hand, numerous researches on CNTs continued since its first discovery; therefore, knowledge and know-how are at more matured level for properties and behavior of CNTs. Furthermore, contributions and synergistically strengthening effects of CNTs to the host materials and overall structures are reported and demonstrated by many researchers.

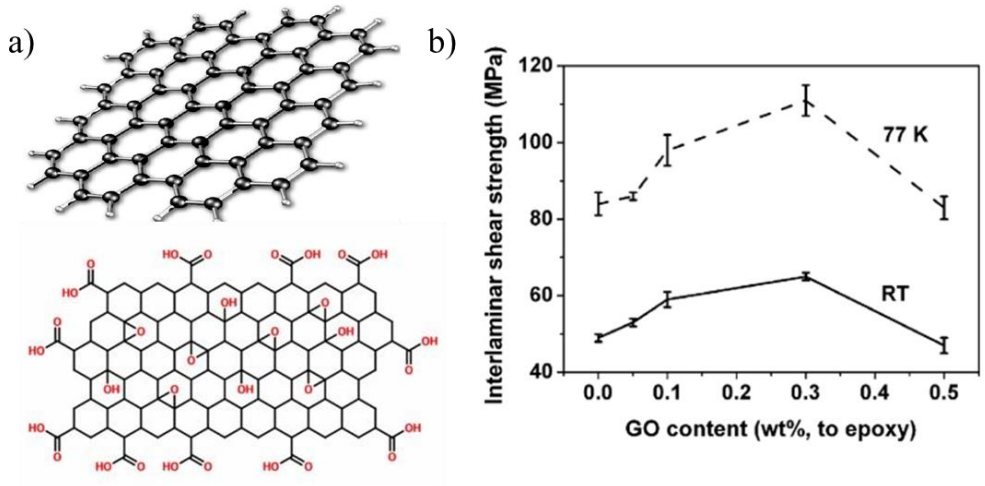

Figure 1.4: a) Schematic illustration of graphene (above) and graphene oxide (below), b) ILSS of glass fiber/epoxy composite reinforced with different graphene oxide weight percentages.

CNTs which is an allotrope of carbon had been first discovered by Ijima in 1990s by using high-resolution cameras [22]. The structure consists of hexagonal bonded graphitic carbon atoms and rolled-up sheets of single-layer carbon atoms (graphene). CNTs have diameters as small as 1 nm and lengths up to several centimeters, which means the structure has high aspect ratio. According to the number of walls, they are categorized as single and multi-walled carbon nanotubes. Single-walled nanotubes (SWCNTs) have one rolled graphene sheet and MWCNTs comprise of several concentrically interlinked nanotubes as shown in Figure 1.5. Depending on number of walls, their physical, mechanical, and thermal properties strikingly differentiate into each other.

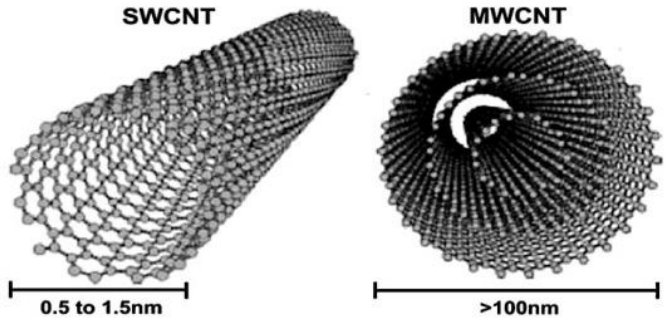

Figure 1.5: Schematic representation of SWCNT and MWCNT [23].

Considering the prominent features of CNTs such as high stiffness and strength, high electrical conductivity, and being the best heat conductive material, they are the subject of many researches with their several forms for several applications as seen in Figure 1.6.

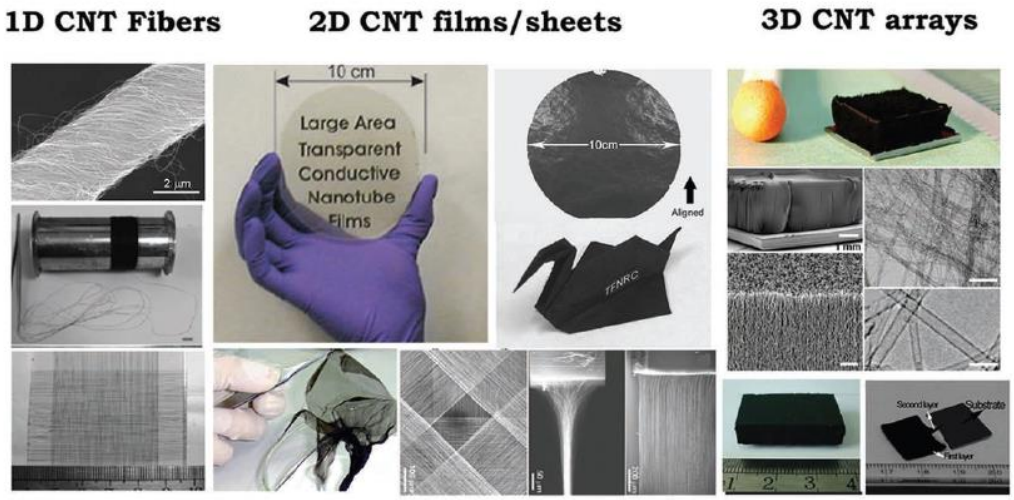

Figure 1.6: Multi-dimensional CNTs for different applications [24].

Polymer nanocomposites (PNCs)

Polymer matrix composites show diversified load carrying characteristic and failure mechanism differently from metallic materials, since they constitute of separate materials. Within the reinforcing techniques of PNCs, the major goal is to enhance the mechanical, electrical, and thermal properties of composites. Distinctive mechanical, electrical, and thermal contributions of nanomaterials to the structure without any weight penalty impel the use of these nanomaterials as reinforcing agents for novel composite materials. Different fillers in multiple forms like particles, fibers, layered structures and clusters are classified as nanotubes, nanofibers, and nanoparticles based on their dimensions and surface area-to-volume ratio. These reinforced composites with nanomaterials are named as polymer nanocomposites (PNCs). PNCs are obtained by homogenously dispersed nanomaterials, which are reinforcing agents having nanoscale dimensions (at least one scale), into the continuous polymer matrix [25]. Sufficient dispersion of exfoliated or intercalated nanostructures into the polymer matrix should be accomplished to achieve promising PNC materials. The most essential concern during fabrication of nanocomposites is the effective dispersion and distribution of nanomaterials. It directly affects the mechanical performances of composites and polymer interfacial areas; wherein the insufficient dispersion of nanomaterials substantially degrades composite performance. Both thermosets and thermoplastics are convenient to properly process with nanomaterials in consideration of processing requirements to fabricate PNCs. For nanocomposite production, solution blending, melt compounding, and in-situ polymerization methods have wide application field among polymer composite processing types, each with its own benefits [26]. Selection of a method for particular part depends on the material, design considerations, and end-use.

The first fabrication method for PNCs is in-situ polymerization, which typically consists of dispersion of nanofillers prior to polymerization process. Saeed *et al.* [27] studied on the conductivity and mechanical properties of polycaprolactone (PCL)/MWCNTs nanocomposites produced by in-situ polymerization. The as-received CNTs (A-CNT) and purified (P-CNT) with nitric acid were dispersed in monomer solution, followed by in-situ polymerization of PCL to form nanocomposites. PCL nanocomposites were characterized via four-point probe

method, TGA, differential scanning calorimetry (DSC) and dynamic mechanical analysis (DMA). It was concluded that besides the improvement of thermal stabilization of polymer with CNT insertion, crystallization temperature was increased due to the CNT induced nucleation zones as seen in Figure 1.7. The enhanced electrical conductivity of composites was achieved with low CNT content for A-CNTs, and uniform dispersion of CNTs was confirmed by rheological data with low percolation threshold (2 wt%).

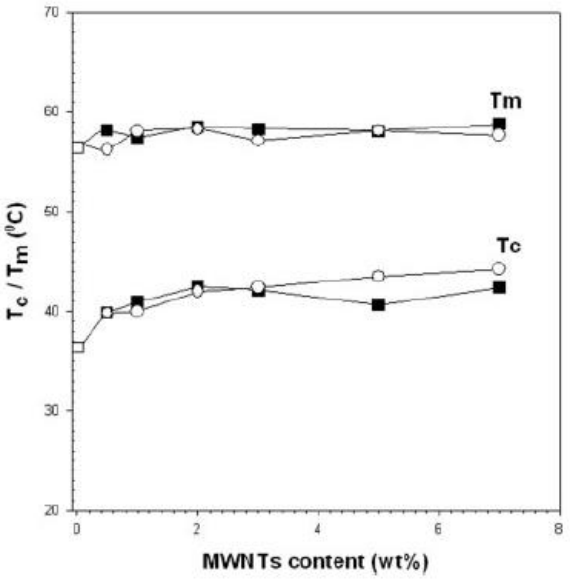

Figure 1.7: Melting and crystallization temperatures of (□)PCL, (○) A-CNT/PCL, (■) P-CNT/PCL with different CNT addition [27].

A common alternative was solution blending, by which nanomaterials were dispersed in solution and the polymer was diluted. Graphene oxide (GO) is one of the nanomaterials incorporating with several kind of polymers. In the study reported by Liang *et al.* [28], GO sheets were exfoliated to individual sheets by sonication in water solution, and were dispersed in poly(vinyl alcohol) (PVA) to form nanocomposite films. Tensile strength, Young's modulus and thermal properties of PVA composites were enhanced even with low concentration of GO. Synergetic effect of nanomaterials even in low weight fractions on both mechanical and thermal properties of the composite was demonstrated. In consonance with thermogravimetric analysis (TGA) results, thermal stability of the PVA was enhanced GO inclusion by regarding the shifts in the peak temperature of the first derivative thermogravimetry curves to higher values as shown in Figure 1.8.

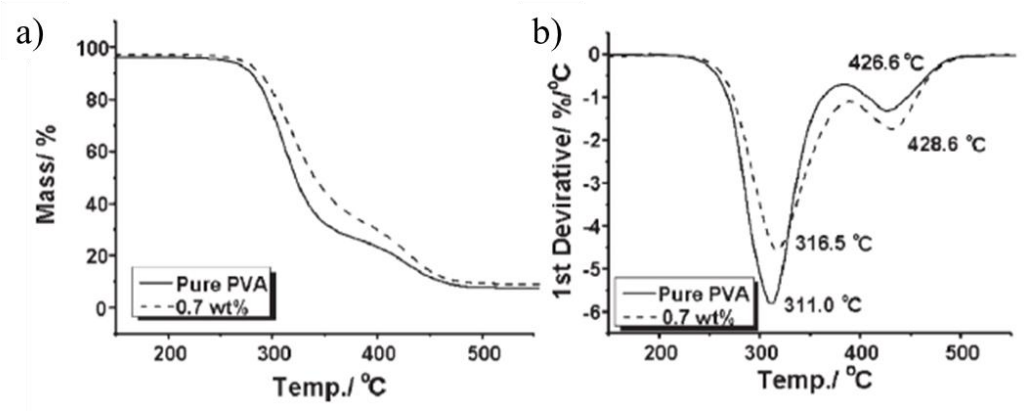

Figure 1.8: a) TGA results of PVA and 0.7 wt.% GO/PVA nanocomposite, b) DTG curve of PVA and its nanocomposite with GO [28].

Reinforcing of polymers with CNTs was extensively performed by solution blending method. Considering the fabrication of CNT reinforced composites from different polymer types, Ajayan *et al.* [29] reported the fabrication of aligned CNT reinforced polymer as an isotropic composite. The dispersion of CNTs into the ethanol solution was obtained from CNT mixture with epoxy resin. Jin *et al.* [30] addressed that the aligned CNTs in specific orientation into polyhydroxyaminoether (PHAE) can be attained by the stretching of nanocomposite at specific temperature after solution blending process.

Ever-increasing demand for faster production rates has pushed the industry to fabricate polymer composites eliminating any chemical process. Melt compounding, also referred as extrusion (Figure 1.9), which referred as a polymer processing method for PMC fabrication, includes melting and blending of thermoplastics with additives to flourish the thermal, electrical, physical, and mechanical features of polymers. Offering cost-effective and time saving solutions for industrial applications, has encouraged researchers to preferentially manufacture most of unique compounds with this method. As stated by Tang *et al.* [31], CNTs were dispersed in high density polyethylene (HDPE) polymer under the shear force applied by twin-screw extruder. It was also verified that a gain in stiffness and fracture toughness were achieved by overcoming the agglomeration issue of CNTs into the matrix. Polymer and nanoadditives were mixed under shear loading at heating zone where two screws concentrically rotate at elevated temperature which was set according to polymer type. While melted polymer passes through the heated barrel, CNTs were simultaneously fed from the same zone. In the co-rotating extruder, screws rotate in the same direction, thus the major part of the polymer was

subjected to the shear loading which ensured homogenous mixing of nanoadditives with polymer. In spite of co-rotating extruder, limited shear force was created in the counter-rotating screws while rotating in the opposite directions, resulting in insufficient dispersion and distribution of additives.

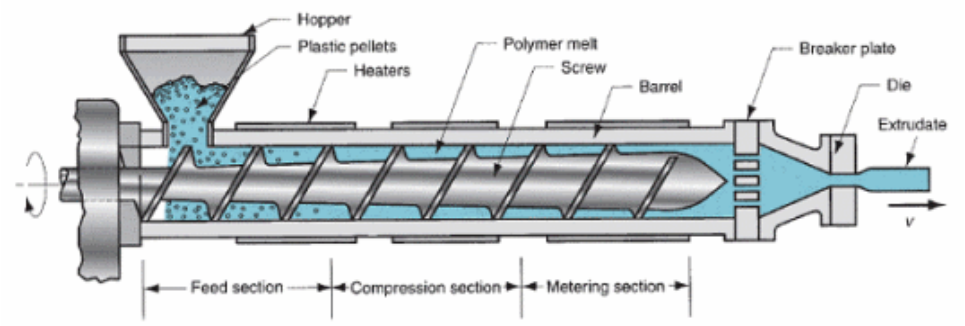

Figure 1.9: Principle of melt mixing mechanism of polymers [32].

Socher *et al.* [33] scrutinized the effect of polymer viscosity on dispersion of nanoadditives, which were MWCNTs in the particular study, for the ultimate nanocomposites. Mixing temperatures of polymers were specified for each type of polymer in three different viscosity levels. The polymers used in nanocomposite fabrication were selected from mass-production and high-performance polymers which were polyamide 12 (PA12), PC and low density polyethylene (LDPE). Improved CNT dispersion and distribution were observed for composites at higher viscosity levels, which indicated that the higher energy input was quite sufficient to achieve homogenous dispersion of CNTs and eventually restrict the formation of stress concentration areas inside the nanocomposite. Highly sufficient dispersion quality of nanomaterials into the polymers was observed in transmission electron microscopy (TEM) images for whole types of polymers. A uniform dispersion of nanotubes was obtained in PA12 (2 wt% CNT) matrix as high viscosity sample (Figure 1.10). Furthermore, only small agglomerations were seen into the low and high viscosity matrices for PC (0.75 wt% CNT) and LDPE (3 wt% CNT) nanocomposites, respectively.

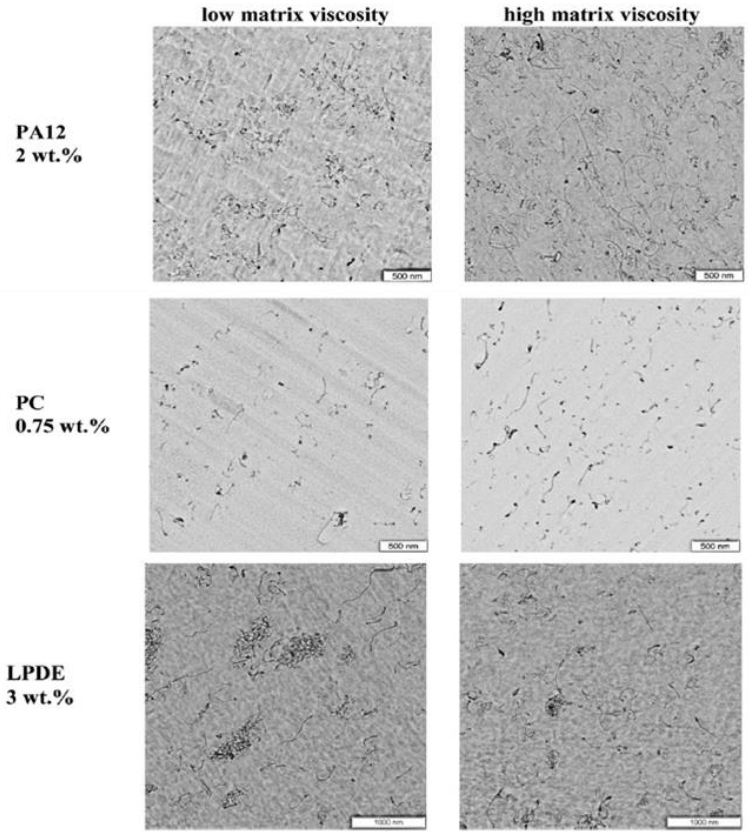

Figure 1.10: TEM images of CNT reinforced PA12, PC, and LDPE [33].

Ferreira *et al.* [34] focused on the correlation between mechanical properties of composites and fabrication process parameters. CNT reinforced HDPE composite was fabricated by compression molding technique following sonication, melting, and mechanical stirring processes. During composite fabrication, the effects of sonication temperature and weight fraction of CNTs on hardness of nanocomposite were examined. Five CNT concentrations (0.1, 0.4, 1.1, 1.8 and 2.1 wt% CNT) and five sonication temperature were combined to reveal the optimum combination according to statistical approach. To get the highest hardness value, optimal sonication temperature (55˚C) and CNT fraction (0.8 wt%) were investigated. According to DSC results, crystalline sites were expanded and crystallization temperature was increased by the insertion of CNTs as shown in Figure 1.11. Mechanical performance, especially hardness of the composite, was enhanced due to the nucleation effect of CNTs inside polymer. These DSC results as well as DMA results provided an insight to link the relation between crystallinity and thermo-physical properties of the composite.

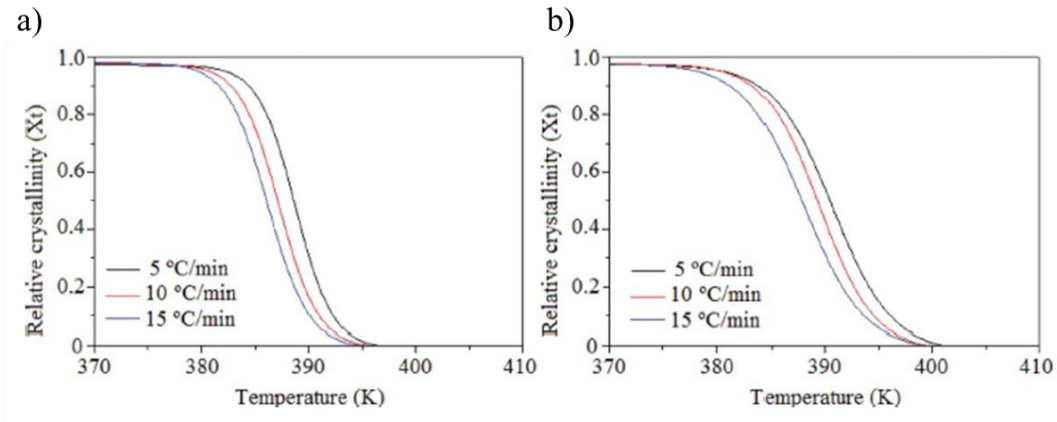

Figure 1.11: Relative crystallinity of a) neat HDPE, b) CNT/HDPE nanocomposite according to temperature at different cooling rates [34].

Mahfuz *et al.* [35] reported that mechanical performance of LDPE composite reinforced with CNTs was improved against to tensile loading. TGA results (Figure 1.12) showed that thermal stabilization of LDPE composite incorporated with CNTs was preserved till 539°C rather than 482°C for neat composite. Moreover, TGA results were verified by X-ray diffraction (XRD) and DSC studies, to prove the mechanical enhancement resulted from the increment in crystallinity level as well as the degree of cross linking of polymer with 2 wt.% CNT infusion.

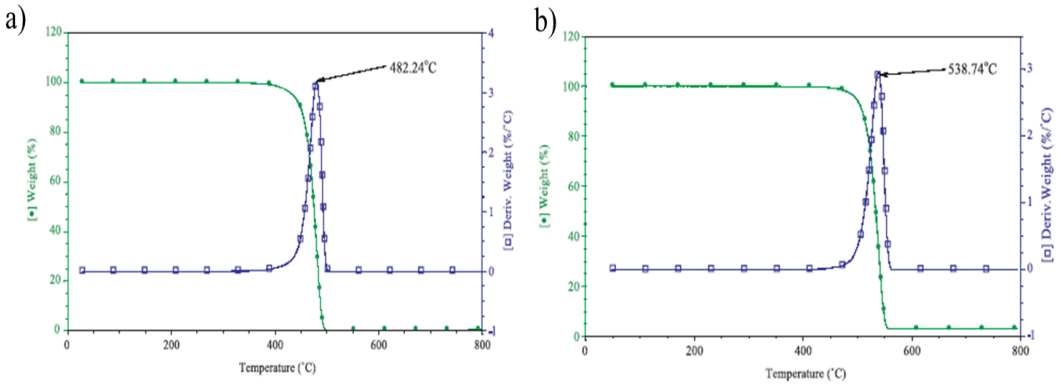

Figure 1.12: TGA thermograms of; a) neat LDPE, b) CNT/LDPE nanocomposites [35].

The brief summary of the studies on PNCs, reinforced with CNTs in literature specifically focusing on the variation of thermal properties of the composites was listed in Table 1.1.

Table 1.1: Literature review of PNCs which contain CNTs as reinforcement.

Matrix	Type of CNT	Method	Characterizations	Results
HDPE	0.1-2.1 wt% MWCNTs	Melt mixing	DSC, hardness test	3% increase in crystallinity [34]
LDPE	2 wt% MWCNTs	Melt mixing	DSC, TGA, XRD, tensile test	57˚C increase in degradation temperature and 37% enhancement in tensile strength [35]
HDPE	1-5 wt% MWCNTs	Melt mixing	SEM, TEM, punch test	Homogenous dispersion of CNTs [31]
Medium Density PE	1.5, 5 wt% SWCNTs	Solution blending	DMA, TGA	8°C enhancement in degradation temperature of PE [36]
PE	0.1-10 wt% MWCNTs	Melt mixing	DSC, TGA	7˚C increase in crystallization temperature of neat PE [37]
PP	1 wt% SWCNTs	Melt mixing	DSC, TGA	Crystallization temperature increased 11˚C and enhanced thermal stability [38]

Reinforcing strategies of laminated composites

Laminated composite is an assemblage of plies consists of high-modulus fibers in different sequences (Figure 1.13). The assemblage is accomplished by heating of laminates and pressing in certain directions. The response and performance of the overall structure distinctly differs on the individual plies, each of which has its own characteristics. Most common and observed failure modes in laminated composites are delamination, matrix cracking, and debonding of matrix and reinforcing agents.

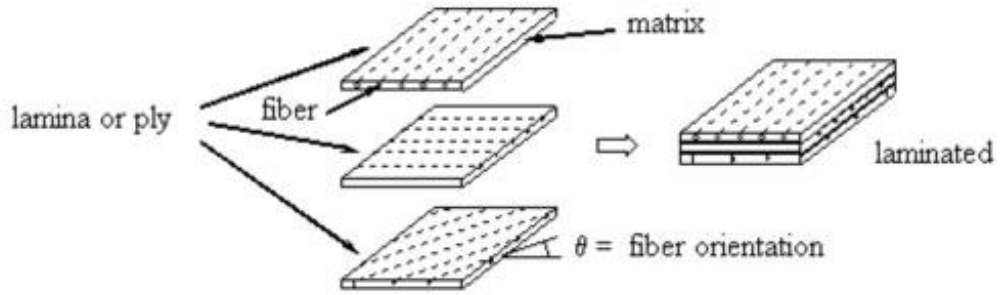

Figure 1.13: Schematic illustration of laminated composites [39].

Interface region of matrix and reinforcement or polymer plies in the composite materials has the possibility to limit efficient load transfer capacity under mechanical loading when the bonding is not well-established in-between. Strengthening of the interface has a crucial role for enhancing the load bearing capacity and microcrack resistance of the overall structure. Considerable research efforts have been devoted to enhance the weakness of laminated composites by implementing various strengthening methods such as z-pinning, matrix toughening, interleaving or stitching. However, this technology is not fully matured yet for primary structures and most of these studies are based on thermoset polymers. Regardless of the material, reinforcement materials are available in diverse forms within films, fibers, nanofibers, and nanomaterials, particularly CNTs, to handle in a wide range of end-use requirements and processes.

One of the reinforcement alternatives to improve the interface is integrating a thermoplastic interlayer which enhances the performance under the loading. Nevertheless, while integrating these materials to the overall structure some challenges could be solved against to incompatibility between reinforcing interlayers and matrix of composites. The study, presented by Stevanovic *et al.* [40] showed that the interlayer, made from poly(acrylonitrile-butadiene-styrene) (ABS) and vinyl-ester (VE) for VE/glass fiber composite, enhanced the toughness of laminates by intensifying the interlocking effect of microcracks through the interfaces. Since there was incompatibility between ABS and VE in terms of plasticity behavior, microcracking was triggered into the resin as a strengthening mechanism.

Apart from the nanomaterials, interleaving of films made from thermoplastics or thermosets are preferred to enhance weak properties of interlaminar region at laminated composites. White *et al.* [41] studied on various interlayers including CNTs, polyamide (PA) and epoxy with different material combinations. Carbon

fiber/epoxy composites reinforced with these interlayers were fabricated by vacuum infusion method. According to the end-notch-flexure (ENF) tests, crack bridging effects and uniform stress distribution through matrix were mostly observed for composites including epoxy/PA and CNTs interlayer. The synergetic effect of hybrid layer made from aramid and phenoxy fiber within carbon fiber reinforced polymer (CFRP) composites was also demonstrated to achieve toughened shear, tensile, and compression properties by Wong *et al.* [42].

The other reinforcing route for laminated composites was braiding which was based on establishing the connection through the composite laminates in the z direction. Within this method, dimensional stability of the structure under static and impact loading were preserved and damage tolerance was also improved compared to conventional laminated composites. This multifunctionality of multidimensional graphite fiber/epoxy braided composite was proven by Crane *et al.* [43].

CNTs in different layered forms such as paper-formed CNTs or interleaf are successfully utilized primarily in laminated composites as strengthening mechanism. The combination of CNTs with laminated composites can be achieved by predominantly three different routes; direct growth of CNTs on the fiber surface to enhance the matrix-fiber interface region [44-48], directly transferring of CNT plies to the composite laminate interfaces after they are grown vertically or horizontally on a substrate surface [49, 50], and interleaving the specific laminate interface of composite with paper-formed CNTs referred to as buckypaper (BP) [51-55].

According to ENF and double cantilever beam (DCB) test results, Veedu *et al.* [48] reported that the remarkable enhancement in fracture toughness and interlaminar shear resistance of silicon carbide (SiC) architectures were incorporated with CNT forest. The improved mechanical performance resulting from interlocking effect of CNTs interface between SiC fabrics was demonstrated in DCB and ENF test graphs as shown in Figure 1.14.

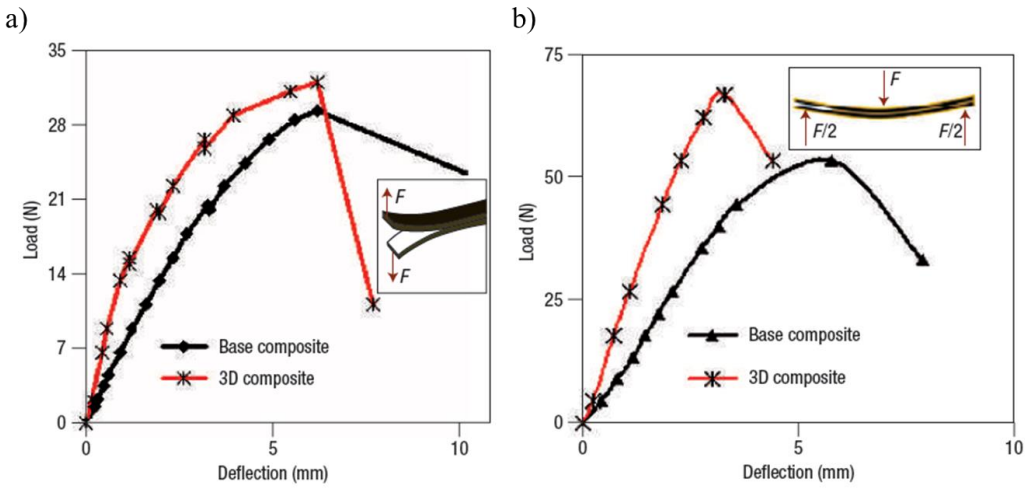

Figure 1.14: Load-displacement curves for neat and CNT reinforced 3D composites from a) DCB, b) ENF tests [48].

In many of reinforcing strategies, another integration route of CNTs is in aligned fashion to accomplish continuous load transferring between plies (Figure 1.15). Direct transferring of CNT plies to the laminates, with preserved alignment, is one of the routes to integrate CNTs layer to the structure subsequently they are grown on substrate. In the study presented by Garcia *et al.* [49], growth CNT plies on silica substrate were transferred to the mid-plane of prepregs for Mode I and II tests to measure the adhesion between carbon fiber and SiC prepreg and fracture toughness. Consequently, the 3-fold augmentation on Mode II fracture toughness was referred to the compatibility between CNTs and prepregs.

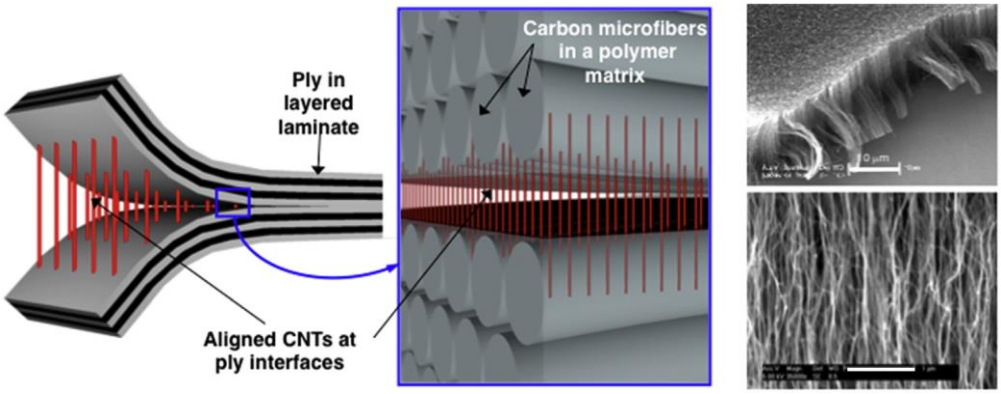

Figure 1.15: Demonstration of CNT bridging effect between carbon and SiC composite plies [49].

Uematsu *et al.* [56] investigated the fracture toughness of PEEK reinforced with carbon fibers according to DCB test results. Unidirectional carbon fiber reinforced PEEK composites were fabricated with different number of laminates and tested at varied temperatures. The increment in fracture toughness at high temperatures was

reported, after the crack propagation behavior and fatigue performance of the composites was evaluated.

Furthermore, carbon fiber was the extensively integrated reinforcement into the polymers to strengthen the interlaminar shear strength (ILSS) [57]. The performed SBS tests indicated that the implementation of chemical and plasma treatment on carbon fibers enhanced the ILSS of CF/PP composites. The wetting of carbon fibers and adhesion with PP films were improved by the attachment of functional groups on carbon fiber surfaces after treatment procedures. As shown in Figure 1.16, 48.7% increase in ILSS of composites justified the strengthened interfacial area between plasma treated carbon fibers and polymer films.

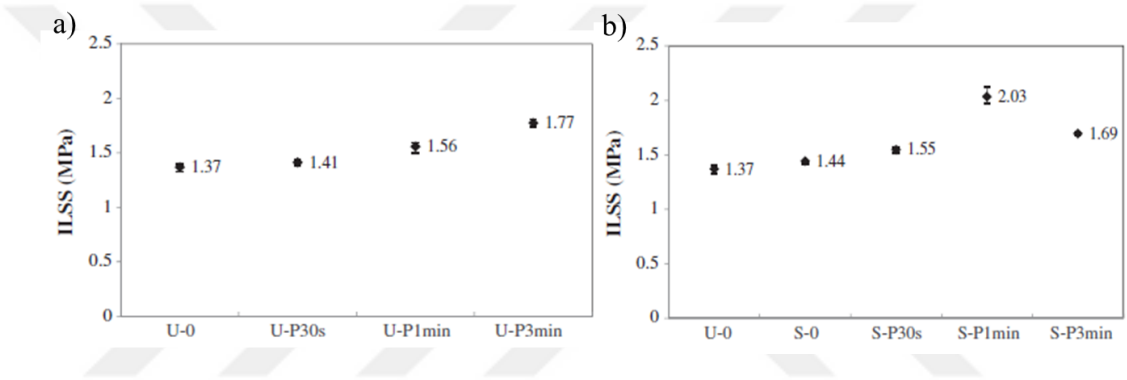

Figure 1.16: ILSS of CF/PP composites depending on surface treatment; a) plasma, b) chemical treatment [57].

As presented study by Wicks *et al.* [46], radially grown CNTs on fibers granted mechanical superiorities to alumina fiber reinforced polymer composites by influencing the load-carrying capacity of the structure (Figure 1.17a). In the research, as an alternative method to z-pinning and stitching, through thickness properties and tension strength of composite were significantly improved depending on CNT pull-out effect. As another approach, Abot *et al*. [50], CNTs were interspersed between plain woven carbon fabrics and subjected to shear, in-plane tensile, and compressive loadings. The enhancements on interlaminar shear stress (ILSS) and tensile strength were achieved by 87% and 16%, respectively when compared with non-reinforced composites (Figure 1.17b and Figure ***1.17***c). Nevertheless, these reinforcing strategies need to complex manufacturing systems such as special designed furnace for chemical vapor deposition (CVD) method to grow CNTs, which causes drawbacks like long fabrication time and high cost. On the other hand, paper-formed

CNTs are simply fabricated by vacuum filtration method without any expense increment for fast industrial applications.

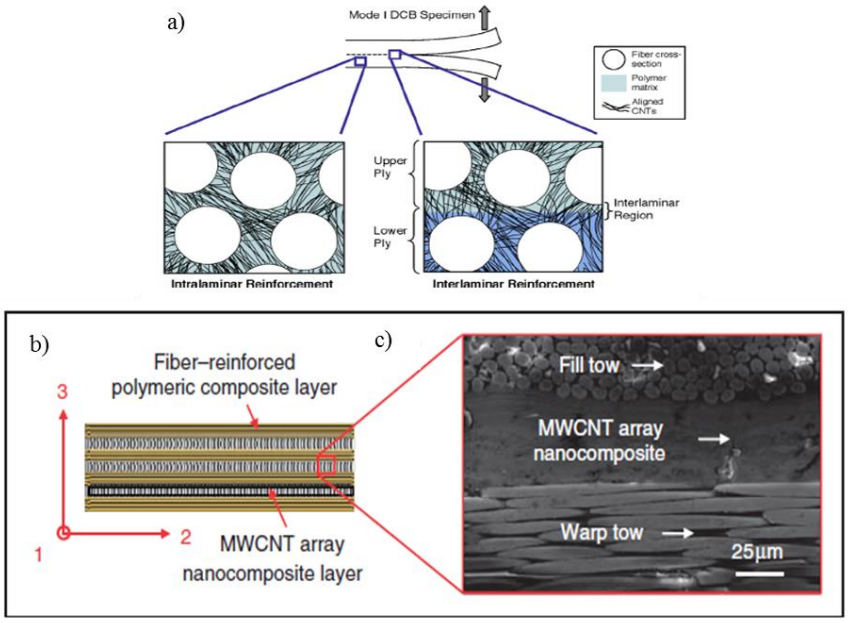

Figure 1.17: Schematic illustration of; a) directly growth of CNTs on fiber surface [46], b) nanolayer reinforced composite , c) SEM image of cross-section of composite [50].

BP can be formed from randomly oriented and highly entangled CNT bundles which interact with each other by van der Waals forces. Several studies are focused on interleaving CNT BP into the composite structures to benefit from its outstanding features like high strength-to-weight ratio, mechanical flexibility, lightweight, and foldability [58].

Through literature survey, it was clearly perceived that multifunctional contributions of BPs into the composite structures were attracted much attention of many research groups, since many studies on this topic were reported. Promising features of BPs in electronic applications were revealed by indicating their significant improvement on the electrical conductivity both in-plane and out-of-plane directions of carbon fiber composite as seen in Figure 1.18, by Wang *et al.* [59]. Though, researches on CNT BP were not restricted only with electrical conductivity of BP in electronic field. In-situ monitoring of delamination within the laminated composites by interleaving with CNT BP, as well as enhancing the delamination initiation stress of carbon fiber composite, were also reported by Liu *et al.* [52]. In their study, carbon fiber/epoxy composite was mechanically and electrically strengthened with CNT BP insertion to

the mid-plane of plies. The change in electrical resistivity was measured simultaneously while being tested under tensile load by acoustic emission method, which enabled detect delamination initiation point by observing stricter alteration in the electrical resistance of BP interleaved composite. Improvement on ultimate strength (3.4%) and the high sensitivity of CNT BPs against delamination has drawn attention by researchers for further applications such as structural health monitoring sensor, recently.

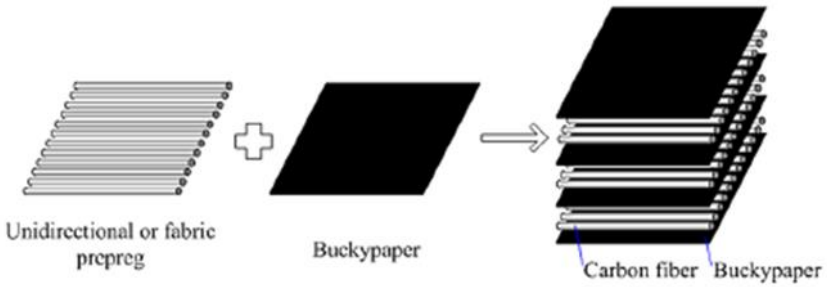

Figure 1.18: Schematic illustration of carbon fiber/buckypaper hybrid composite [59].

Based on functionality of CNT BP as a sensor, there are some other researches on the utilization of CNT BP as a tensile strain sensor [55] and a monitor to track the curing behavior of polymer [60]. Tensile strain response of composite can be controlled by embedding BP to the glass fiber reinforced epoxy composite owing to the exceptional piezoresistivity of CNT BPs [55]. Lu *et al.* [60] utilized BPs for feasible applications with their study to show that highly flexible BP allows to measure the change in resin phase in real time.

Besides its use in sensing applications, CNT BPs are also preferred to enhance the weakness of the interface region of laminated composites. DCB and ENF tests can be used to achieve a deep knowledge about interlaminar fracture toughness of composite and quality of interfacial bonding. A recent paper published by Liu *et al.* [54] investigated the bridging effect of CNT BP interleaf on Mode I and Mode II fracture toughness of carbon fiber reinforced composites. The mechanical performance of laminated composite is highly dependent on the thickness of CNT interlayer, likewise stacking sequence of plies. The correlation between thickness of CNT films into the carbon fiber composite and associated mechanical properties of structure was evaluated by Li *et al.* [61]. The effect of intercalated thin and thick CNT films in composite structures on ILSS also tensile and compressive strengths

were assessed by conducting several mechanical tests. The decrement in ILSS for thicker CNT film revealed that thicker CNT layer degraded physical compatibility of interfaces of prepreg plies. In spite of thicker CNT film, ultrathin CNT film slightly increased (5%) the ILSS as shown in Figure 1.19. On the other hand, compression strength was strikingly improved by 34% by dissipating energy between CNT bundles and their connection nodes.

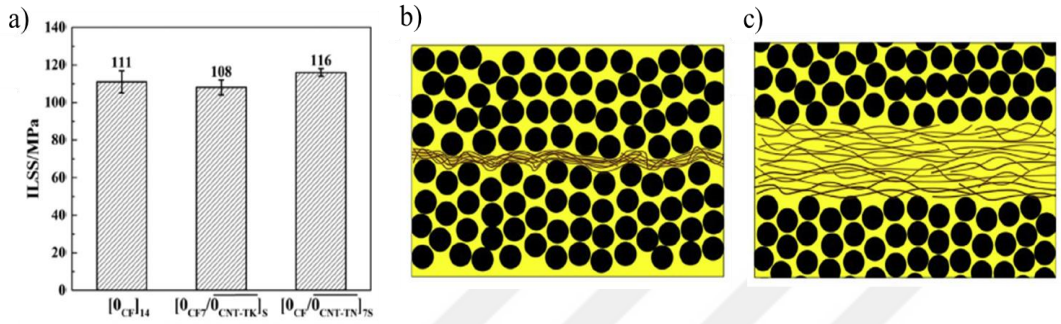

Figure 1.19: a) ILSS values of neat CFRP composite and reinforced with thin and thick CNT BP respectively, schematic illustration of composites with; b) thin CNT BP, c) thick CNT BP [61].

In addition to thermoset composites, significant efforts are devoted to integrate CNT BPs into thermoplastics to improve their mechanical and electrical properties, fire retardancy and electromagnetic interference performance. Contrarily to thermoset composites, thermoplastic laminated composites are not formed by a chemical reaction and require only a heating procedure, which is the primary preference for existing routes of fast implementation. Effective consolidation has critical role on efficient energy absorption of individual laminates for specifically design of armor materials and bulletproof vests. The response of the overall structure under loading is specified by the quality of consolidation and orientation of plies [62]. As reported and applied in several experimental studies, the most common laminated composite fabrication method preferred for thermoplastic polymers is compression molding also referring to hot press method. Laminated composites are broadly fabricated by this method in which a high pressure is applied to the preheated polymer for consolidation. Simply embedding of reinforcing layer between the polymer plies and straightforward manufacturing steps accelerated the preference of this method for composite fabrication, despite the void risk and low output rate [1].

Mechanical properties of CNT BPs such as the ultimate tensile strength, elongation at break and fracture toughness were enhanced by thermoplastic polyurethane (TPU)

impregnation at proper volume fraction as seen in Figure 1.20 by using vacuum filtration method [51]. During thermoplastic composite fabrication, the main challenges are wettability issue of BPs and insufficient adhesion between polymer layers and CNT BP layer. It is well known fact that interfacial properties of laminates play a crucial role to achieve high performance composites. To overcome these drawbacks, researchers have developed many methods for CNT BPs such as ozone and plasma treatment or microwave irradiation for efficient interfacial bonding. Among these methods, Qu *et al.* [63] reported that treated CNT BP by microwave irradiation process provided prominent enhancement in tensile strength and chemical compliance due to the effective interfacial bonding between polyethylene (PE) laminates and CNT BPs. When CNT BPs are inserted to the structures, high elongated thermoplastics could act in a more brittle behavior. Hindering of this deteriorating feature is possible by exposing CNTs or polymers to such additional modification processes and these studies proved the favorable effect of treatments on mechanical improvement.

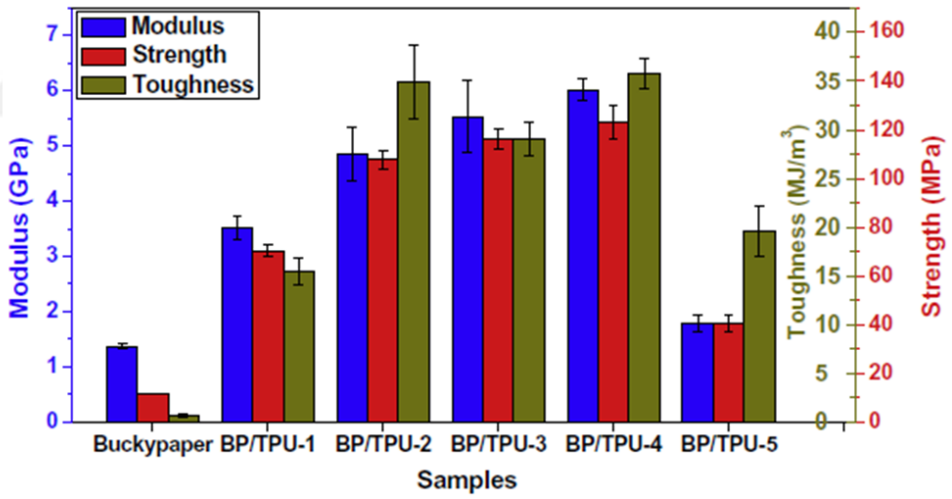

Figure 1.20: Tensile test results of as-prepared BP and CNT BP/TPU composites with different volume fractions of TPU resin [51].

Besides their exceptional mechanical performance; excellent electrical conductivity and high aspect ratio of CNTs make them promising candidates for electromagnetic interference (EMI) shielding material in multifunctional composites. Laminated LDPE composite reinforced with CNT BP interlayers was manufactured at slightly above the melting temperature of LDPE by vacuum bagging method to compare with polymethacrylimide (PMI) foam and CNT BP reinforced laminated epoxy composite

in terms of EMI shielding (Figure 1.21) [64]. Consequently, they reported that there were limitations about the number of intercalated CNT layer and proper stacking sequence to obtain efficient EMI shielding.

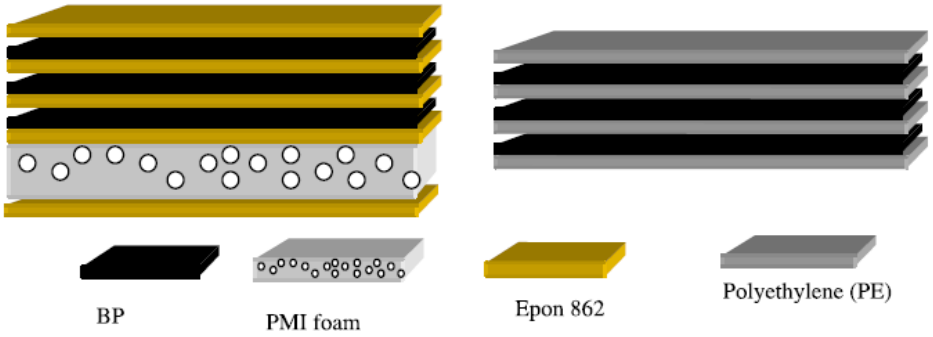

Figure 1.21: Schematic illustration of laminated composite in different sequences [64].

The alignment was performed on the randomly oriented CNT bundles by pre-stretching before insertion to the structure; therefore, improved tensile properties and load carrying capability could be obtained in the specified direction. Li *et al.* [53] studied on aligned CNT BP inserted polyphenylene composites with the motivation of combined high mechanical, electrical, and thermal performances of multifunctional composites. One of these multifunctional properties of CNT BP is its resistance to flammability. Reducing the flammability of thermoplastics with CNTs has considerable importance especially in aerospace industry for cabin filtration systems and airworthiness. In the study about fire and flame retardancy of polyimide, which is one of high-performance plastics, CNT BP was integrated on the surface of polyimide/carbon fiber composite for high-temperature applications and significant reduction on smoke was reported by Fu *et al.* [65]. According to TGA results (Figure 1.22), mass loss of composite during combustion was reduced owing to high surface area and thermal stability of CNT BP. This favoring advantage of CNT BP improved the fire retardancy of polyimide by increasing the thermal stability of polymer.

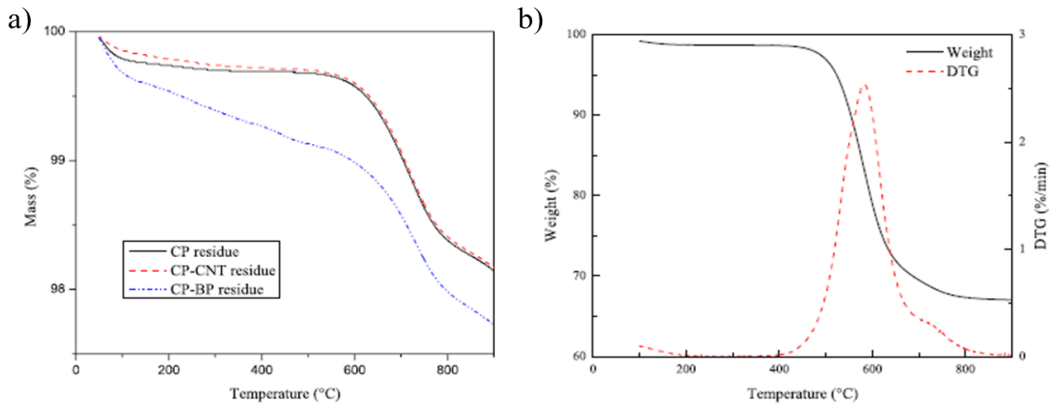

Figure 1.22: TGA thermograms of; a) neat carbon fiber composite (CP), CNT reinforced carbon fiber composite (CP-CNT), CNT BP reinforced carbon fiber composite (CNT-BP), b) neat polyimide [65].

In the presented study, laminated composites are fabricated from ultra-high molecular weight polyethylene (UHMWPE), as a member of semi-crystalline thermoplastics is a third generation material after carbon and aramid fibers with extremely high C_2H_4 molecular mass, greater than 1 million g/mol. The high-performance polymer consists of extremely long polymer chains as shown in Figure 1.23, is used in worldwide markets and wide range applications among thermoplastic polymers [66]. Over the past decade, several studies on UHMWPE composites have revealed that UHMWPE has superior features as high specific strength (40% higher than aramid), durability, excellent impact toughness even at extremely low temperatures by efficiently spreading out energy along the fiber direction, high resistant to corrosive chemicals and exceedingly low moisture absorption. The advantage of recyclability without any further required process to separate fibers and the matrix enables its use in fast industrial processing. These superior properties grant new advantages to several applications ranging from ballistic [67-69] and medical [70] to aerospace [71].

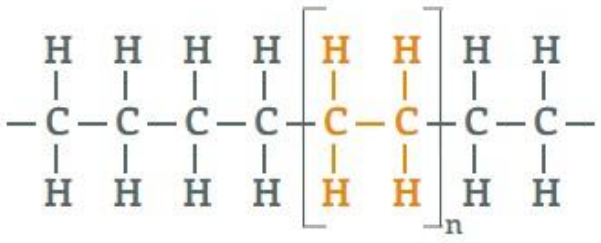

Figure 1.23: Chemical structure of UHMWPE [72].

Besides the prominent ballistic performance of UHMWPE fibers and laminates; high strain rate effect on tensile response of fibers, yarns, and laminates was studied by Russel *et al.* [73]. The comparison of UHMWPE composites with CFRP composites was investigated by Karthikeyan *et al.* [69] under static and dynamic loading. It was concluded that UHMWPE structures performed better than CFRP composites. Ronca *et al*. [74] documented on the enhancement of tensile strength and modulus of UHMWPE by tailoring the molecular structure of polymer with SWCNTs. [75-77]. According to the supplied data by Teijin [78] and Atli-Veltin's study [79], UHMWPE films tend to protect the load carrying capacity and become stronger at cryogenic temperatures compared to their counterparts in room temperature environment which is a desired property for cryogenic applications. Despite the excellent mechanical performance of UHMWPE films under tensile loading, low shear strength and modulus between UHMWPE plies have been reported by Atli-Veltin as shown in Figure 1.24.

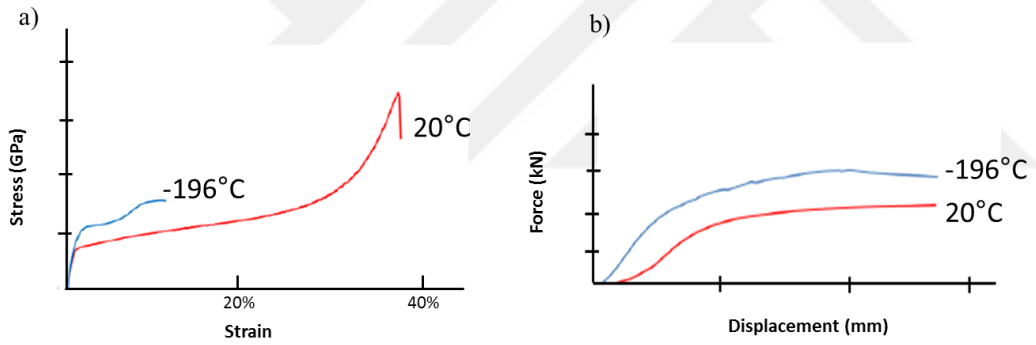

Figure 1.24: Test results for Endumax® at room and cryogenic temperatures; a) tensile test results, b) SBS test results [79].

1.2 Motivation

Many industrial fields such as aerospace, energy, and automotive industries are seeking clean energy sources, which addresses researchers converting energy systems from fossil fuels to zero waste and renewable sources. Cryogenic substances meet these demands particularly from aerospace industry for storage of LH_2 and LOX as rocket fuels also from energy industry in order to transport and store LNG. While operating these materials, structural parts are directly exposed to such extremely low temperatures resulting from cryogenics; therefore, these structures should withstand and maintain their thermal stability under huge thermal cycling. Heretofore, impressive investments is devoted to replace metallic cryogenic tanks

with carbon fiber reinforced thermoset composites; nevertheless, this attempt brings about some drawbacks like brittleness at low temperatures, occurrence of leakage between constituents during thermal cycles, and being non-recyclable. Consequently;

- In this study, SPCs made from chemical resistant, high strength, and recyclable UHMWPE are proposed as an alternative material to metallic materials and also solutions for leakage in between composite structures and catastrophic failure of these systems.
- Despite of the fact that these UHMWPE films have excellent tensile properties, they show lower shear performances compared to other materials. This drawback of the material reveals that enhancement of the shear performance of this material is a mandatory focusing area by adjusting interfacial properties with nanomaterials.
- The main aim of the thesis is to improve interlaminar shear strength of UHMWPE composites by taking advantage of the bridging and interlocking effects of CNTs between laminates, which prevent and delay crack propagation through interlaminar area of composite as well as mechanical improvement on structure.
- UHMWPE composites interleaving with easily processable CNT films are tested under shear loading at room and cryogenic temperatures to evaluate their feasibility for cryogenic applications.
- Besides evaluation of the mechanical properties for fabricated laminated composites, thermal behaviors of these composites as well as CNT interlayers are systematically examined after they are exposed to extremely low temperatures.

1.3 Research Road Map of Thesis

CNT reinforced UHMWPE laminated composite is fabricated and characterized for cryogenic applications, with regards to the feasibility of UHMWPE films for cryogenic structures, and their enhancement with CNTs on overall structure at especially in cryogenic environment. Scope of the thesis is described as the fabrication of CNT films and their polymeric composites followed by performing their mechanical tests and thermal analysis for both composites and CNT films. Two

different types of CNT interlayers are fabricated by using two distinct manufacturing methods. First approach is integration of paper-formed CNTs which are manufactured by vacuum filtration method. In this method, MWCNTs are dispersed into ethanol solution by ultrasound sonication with four different weight percentages that directly affect CNT BP thickness and eventually mechanical behavior of the overall composite. The second approach for strengthening the composite is the fabrication of HDPE thin films reinforced with MWCNTs. HDPE granules are melted and fed with CNTs through twin-screw extruder, then pressed under high pressure and temperature to obtain the desired materials. After insertion of CNT films into the mid-plane of UHMWPE films, these laminates are compressed and molded to achieve laminated composite structures. Shear performance of the composites are evaluated via short-beam shear tests at room and liquid nitrogen environments. Liquid nitrogen environment is created by building up a chamber which surrounds the test mechanism and filled with liquid nitrogen. Experimental road map of the thesis illustrating these fabrication processes is shown in Figure 1.25. Then, thermal and morphological analyses are conducted to link the change between crystalline structure of materials at extreme environment and their mechanical performances.

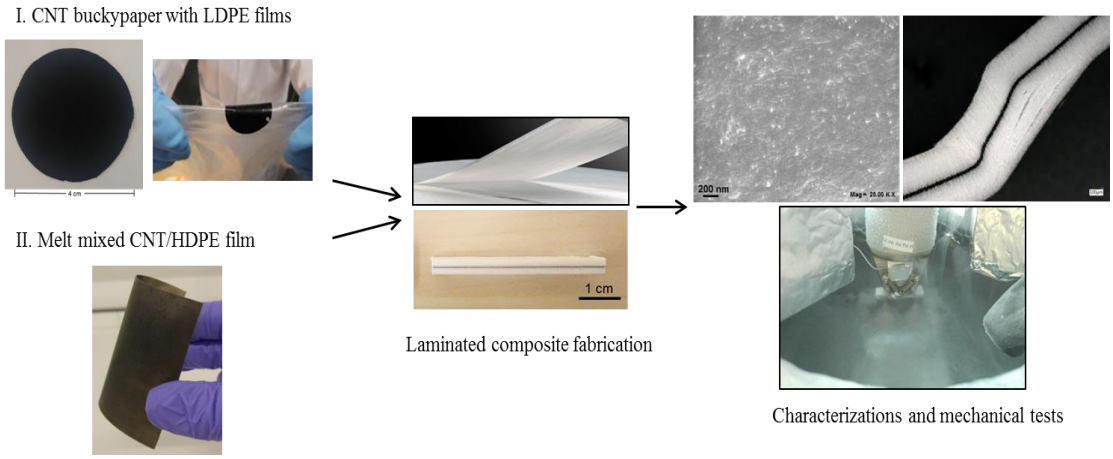

Figure 1.25: Road map of thesis from CNT film and composite fabrication to characterizations.

2. MATERIALS AND METHODS

Fabrications of CNT BPs in different CNT weight percentages, CNT reinforced HDPE films, and UHMWPE laminated composites are described in addition to their thermal and morphological characterizations, and mechanical tests.

2.1 Materials

2.1.1 Carbon nanotubes (CNTs)

In this study, MWCNTs are used as reinforcing fillers for both CNT BPs and melt mixed CNT/HDPE film manufacturing. MWCNTs are commercially purchased from Sigma-Aldrich. They have 98% purity, an outer diameter of 10 nm ± 1 nm, an inner diameter of 4.5 nm ± 0.5 nm and a length 3-6 μm.

2.1.2 Ultra-high molecular weight polyethylene (UHMWPE)

Laminated composites are made from UHMWPE film which is obtained from Teijin Aramid in The Netherlands with a commercial name, Endumax®. In the data sheet [78], it is stated that the density is 0.97 g/cm3, tensile modulus is 170 GPa and elongation at break is 1.7%. This film is made from compaction of UHMWPE powder consisting of extremely long chains of $(C_2H_4)_n$. Then, the thickness of the film is reduced by stretching and rolling until the desired thickness is achieved (between 50 and 60 μm). During these processes, polymer chains become highly aligned, which enhances the mechanical properties of these films and UHMWPE and HDPE films show a characteristic which is bonding well to each other. Therefore, to promote the adhesion between polymer laminates, Endumax® films are provided with a bonding surface by manufacturer, which is a HDPE film as seen in Figure 2.1.

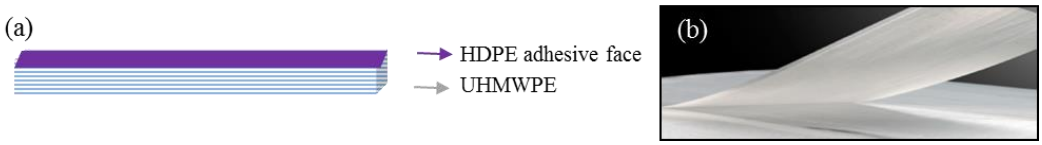

Figure 2.1: Endumax film; (a) schematic illustration, (b) real appearance.

2.1.3 High density polyethylene (HDPE)

The second type of CNT core layers are fabricated from HDPE granules, which are bought from Jam Petrochemical Company. The HDPE granules have 1359 MPa flexural modulus and 25 J/m notched izod impact resistance [80].

2.2 CNT Reinforced Composite Fabrication

2.2.1 CNT buckypaper (CNT BP) fabrication

Parametric studies are performed to evaluate the effect of CNT BP interlayer thickness on mechanical characteristics of overall structure. Mainly two procedures are carried out while fabricating CNT BP; CNTs are dispersed in the solution which is followed by the filtration of CNT suspension through the filtration paper with the aid of the vacuum. Dispersion of CNTs in a solution is still challenging because of their van der Waals forces creating a strong interaction between CNT bundles. Selection of the proper dispersion media and procedure has a crucial role to overcome any agglomeration of CNTs inside the structure. Up to date, several dispersion media are studied to achieve effective CNT dispersion. Liu *et al.* [52, 54] dispersed non-functionalized and acid functionalized CNTs in dimethylformamide (DMF) solution. As an alternative to DMF or other solvents, water is another potential media where surfactants are added to obtain a homogenous dispersion of CNTs in the solution [51, 55, 81]. However, when CNTs are dispersed by using additional chemical agents such as surfactants, it is usually difficult to remove surfactant molecules from product where the chemical and mechanical properties may be affected [81-83]. Besides water and other solvents, ethanol is widely used for dispersion owing to its low temperature evaporation capability, surfactant-free processes [84] and its high suspension stability [85]. As another approach, it is revealed that suspension stability of nanofillers and dispersion media are directly related with zeta potential of the solution which refers to dispersion and stationary of nanoparticles in the mixture. Zeta potential explains electrostatic repulsion forces, arising from surface charge of fillers, between bundles and solution. High absolute value of zeta potential indicates a more homogenous dispersion wherein particles are not in a tendency to agglomerate. The presented study by Ma *et al.* [85] investigated the effect of solution media on dispersion state with different types of functionalized

CNTs by ultraviolet/ozone treatment and zeta potentials that can be viewed in Table 2.1.

Table 2.1: Zeta potentials of water, ethanol, and hexane with different CNTs [85].

	CNT-A (mV)	CNT-B (mV)	CNT-C (mV)
Water	-(24.8 ± 2.2)	+(10.3 ± 1.4)	+(19.8 ± 1.8)
Ethanol	-(18.0 ± 3.5)	-(26.3 ± 10.8)	-(44.4 ± 7.0)
Hexane	-(10.4 ± 5.4)	+(6.18 ± 4.0)	+(19.3 ± 9.2)

Researchers deduced from various visual and morphological examinations that the state of dispersion stability is directly correlated with zeta potential results as seen in Figure 2.2. According to high absolute zeta potential values and favorable dispersion stability, ethanol would be the promising solution media instead of water or hexane.

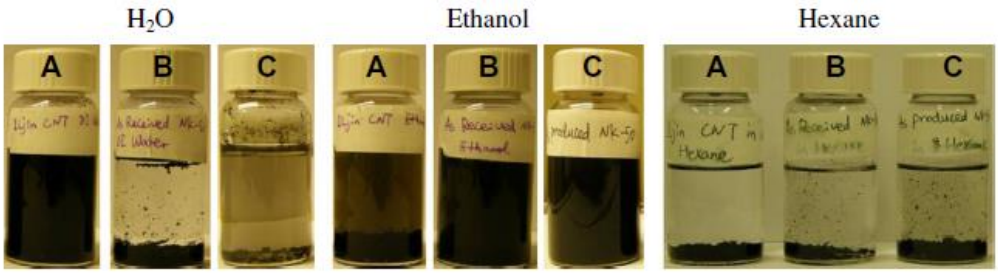

Figure 2.2: Suspension stability of different CNTs in different solutions after 30 min (right: water, middle:ethanol, left:hexane) [85].

In this study, various weight fractions ranging from 0.05 to 0.2 wt.% of CNTs are dispersed in 100 ml of ethanol by ultrasound sonication (VC505/VC750, Sonics & Materials, Inc.) at 60% amplitude for 15 min. CNT dispersed ethanol solutions are filtered through a 47 mm diameter sized polytetrafluoroethylene (PTFE) membrane filter (Whatman®) with a pore diameter of 0.45 μm by a vacuum filtration system as shown in Figure 2.3a. Followed by the filtration process, the filtered CNT BP is kept in an oven at 55°C for 24 hours to obtain completely dried CNT BP and peeled from the membrane. No surface modification or purification is applied to the CNT BP which provides an easy and time-efficient production for both scalability and industrial compatibility. The final product of this process is shown in Figure 2.3b. CNTs network is observed without any significant agglomerations as shown in Figure 2.3c with an image by scanning electron microscopy (SEM).

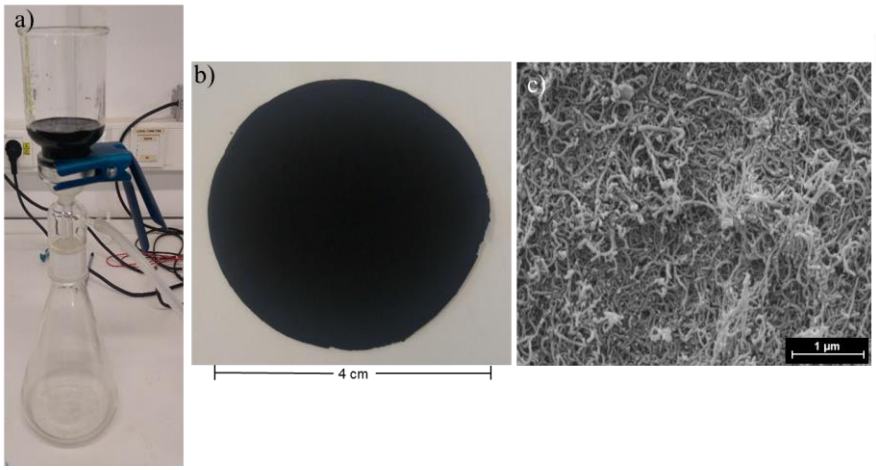

Figure 2.3: Fabrication of CNT BP; a) by vacuum filtration of CNT/ethanol solution, b) filtered and dried CNT BP, and c) SEM image of CNT BP.

2.2.2 CNT/HDPE film fabrication by melt mixing

Besides CNT BPs, CNT/HDPE film is fabricated as an alternative interlayer to be integrated to thermoplastic laminated composites in comparison with CNT BPs. HDPE granules are melted and mixed with a weight fraction of 0.2 % MWCNTs through a twin-screw extruder at 165°C with 65 rpm rotation speed of screws. Neat and extruded CNT reinforced HDPE granules are presented in Figure 2.4.

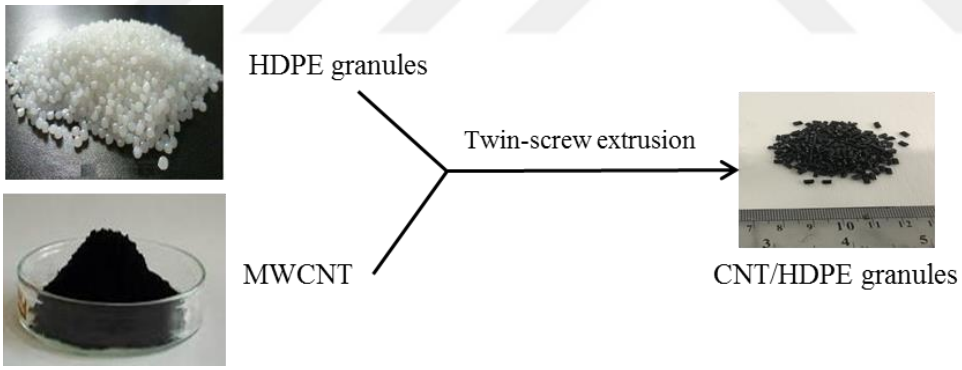

Figure 2.4: Extrusion process of MWCNTs and HDPE granules.

Dispersion and distribution of CNTs are ensured after five extrusion cycle with a specific twin-screw extruder shown in Figure 2.5 in detail. Following the mixing process, reinforced pellets are heated to 200°C under vacuum to remove residual moisture into the polymer granules. Then CNT/HDPE pellets are pressed in the mold at high temperature (190°C) and pressure (20 bar), the compression process results in 4 mm thick nanocomposite.

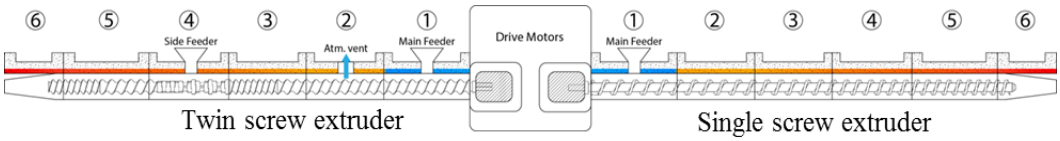

Figure 2.5: Schematic illustration of single and twin-screw extruder.

The melt mixed polymer nanocomposites of CNT/HDPE are later pressed at 200°C and 25 kN by two times to achieve films having homogenous thickness as thin sheet and then placed between composite plies as a thin layer (~200 μm in thickness) which is measured by high sensitivity micrometer (Figure 2.6).

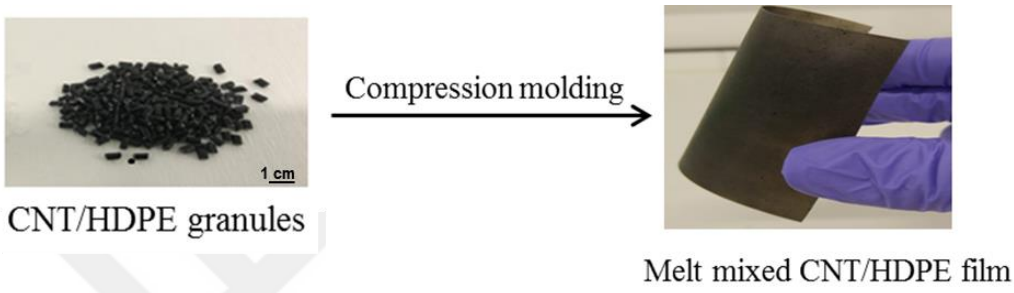

Figure 2.6: Compression molding process of CNT/HDPE granules.

2.2.3 CNT reinforced laminated composite fabrication

Uniform composite structure with a reinforcing interlayer is a critical concern during manufacturing processes. The surface interaction of nanofillers with polymer has to be guaranteed as much as large to ensure continuity of load transferring through the thickness. Within the composite fabrication, the most critical parameter is to achieve sufficient impregnation of BPs at various thicknesses with polymer. Prior to composite fabrication, additional polymer layers such as LDPE and HDPE are used to overcome the bonding issue of UHMWPE resulting from hydrophobic character of polymer. Both LDPE and HDPE films are added to the structure and these polymers are from same chemical family with UHMWPE. There are several parameters that play role in this step. Hence multiple options are taken into account to optimize manufacturing steps.

Process variables can be summarized in four main parameters which are:

- Type of adhesive layer to be placed above and below the CNT BP (HDPE or LDPE),
- Number of LDPE layers pressed with CNT BPs in different thicknesses,
- Compression molding parameters of CNT BP/LDPE layers,

- Endumax® sequences (HDPE bonding side points upwards or downwards).

In addition to compression molding technique, RPS-L belt laminator (Figure 2.7) is also used for LDPE and CNT BP integration at 160°C with 10 kN. However, sufficient bonding is not achieved between polymer and CNT layers through this method.

Figure 2.7: Belt laminator for composite fabrication.

After determination of using hot press machine (Fortijne Presses) for composite fabrication, process parameters are optimized while integrating additional polymer layers to the CNT BPs. According to morphological analysis conducted with SEM and optical microscope, LDPE film shows better compatibility rather than HDPE films, due to its lower viscosity and melting temperature. The number of LDPE films is adjusted by taking into account the difference of various CNT BP thicknesses. Therefore, in order to achieve efficient wetting and adhesion, CNT BPs having 0.05 and 0.065 wt.% CNTs are pressed by placing 6 layers of LDPE films above and below the BP layer. For 0.13 and 0.2 wt.% CNT BPs which are thicker, 8 layers of LDPE films are used below and above of CNT BPs. As a first step of composite fabrication, LDPE/CNT BP/LDPE layers are compressed at 220 °C and 20 kN which is resulted in a highly flexible CNT BP and polymer film as shown in Figure 2.8.

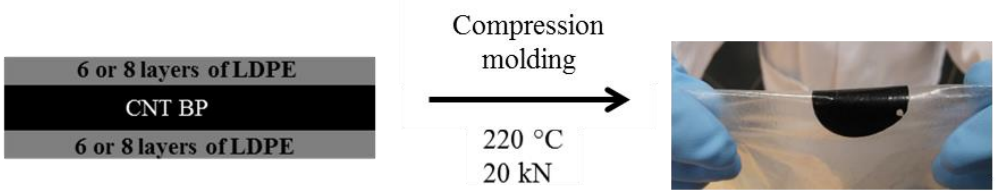

Figure 2.8: Laminated composite design with CNT BP/LDPE interlayer in symmetrical configuration.

Laminated composites are compressed at specific temperature and pressure by using hot press machine (Figure 2.9) at Teijin Aramid manufacturing facility. Subsequent to the compression of CNT BP and LDPE films, these bonded layers are laid and inserted into the middle interface of the 60 Endumax® plies to achieve specific thickness as stated in the test standard (Figure 2.10). Within the laminate, all HDPE bonding faces of the Endumax® films point downwards.

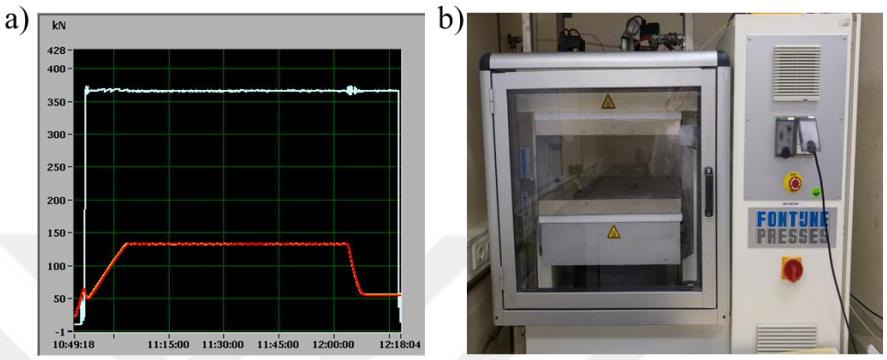

Figure 2.9: a) Temperature and pressure profiles of compression molding, b) hot press machine.

Figure 2.10: Laminated composite design with CNT BP/LDPE core layer in symmetrical face sheet configuration.

Similar to CNT BP/Endumax® composite fabrication explained above, melt mixed CNT/HDPE film is also placed to the middle interface of the 60 Endumax® plies and compressed at same temperature CNT BP/Endumax® composites (Figure 2.11). The HDPE sides of Endumax® films directly interact with the melt mixed CNT/HDPE film for efficient adhesion between CNT film and polymer plies.

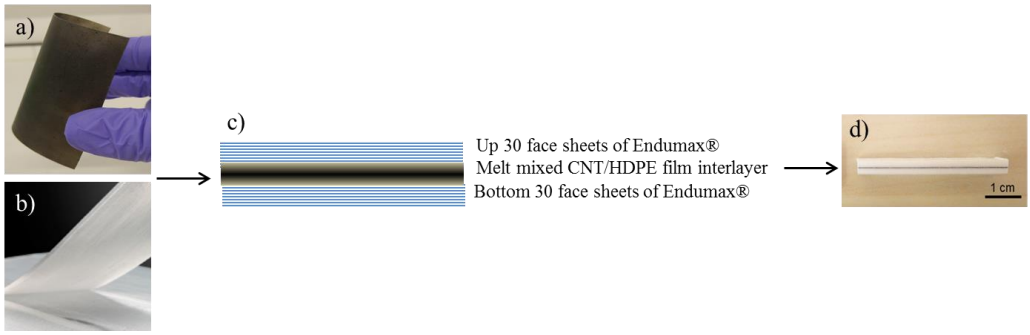

Figure 2.11: a) Melt mixed CNT/HDPE film for core layer, b)Endumax® film, c) laminate design and d) final laminated composite.

All composites are cut by FlowCut Waterjet Cutting B.V. with water jet in the specified dimensions as shown in Figure 2.12. Dimensions of specimens are based on ASTM D2344 standard [86] and the study of Adams [87].

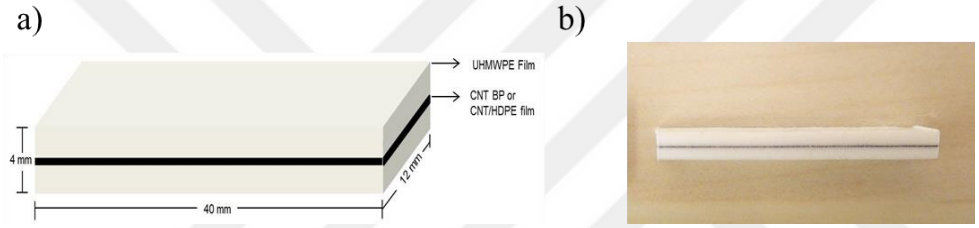

Figure 2.12: a) Dimensions of final laminated composite and b) final laminated composite cut by water jet.

Specimen types and detailed information about manufacturing of composites are summarized in Table 2.2.

Table 2.2: Summary of specimen naming and manufacturing details.

Name of specimen	wt.% CNT	Adhesion film	Number of films	Thickness of CNT film (μm)
Neat	-	-	-	-
Melt mixed CNT/HDPE film*	0.2	-	-	180
CNT BP**	0.05	LDPE	6	150
CNT BP**	0.065	LDPE	6	220
CNT BP**	0.13	LDPE	8	518
CNT BP**	0.2	LDPE	8	709

* Melt mixed CNT/HDPE film as core layer.
** CNT buckypapers at different weight fractions as core layer.

2.3 Characterizations and Mechanical Tests

2.3.1 Thermal analysis

Differential scanning calorimetry (DSC)

Differential scanning calorimetry (DSC) is a thermoanalytical analysis, to specify thermal phase transitions of materials. This technique is based on the measurement of heat flow which is required to increase the temperature of specimen. Thermal behavior of materials such as heat releasing and change in enthalpy are precisely related with the crystalline structure of the materials [88]. A wide range of materials including polymers, chemicals, composites, metal alloys and organic materials *etc*. are analyzed by using DSC to identify their chemical structures. As specific outcomes, DSC analyses give crystalline, onset, offset and glass transition temperatures as well as enthalpy change. These terms are also used to describe manufacturing details and phase transition related to crystalline and amorphous regions of the material [89]. TA, DSC250 equipment is used to carry out the analyses where the specimens are heated from 25°C to 220°C with 10°C/min heating rate in three cycles which are heating, cooling, and reheating. The latest cycle is critical to restrict the movement of polymer chains. Particularly, the change in chemical structure of melt mixed CNT/HDPE films is analyzed by this method in order to develop a deeper knowledge on the effect of extremely low temperature (LN_2) during mechanical testing.

Thermogravimetric analysis (TGA)

Thermogravimetric analysis (TGA) is a thermal analysis for thermal stability characterizations of materials by controlling the change in the mass of specimen as a function of increasing temperature, under controlled environment. In ambient chamber, which is filled with nitrogen or another inert gas to avoid any chemical reaction between specimen and environment, specimen is heated up to elevated temperature meanwhile mass variance is tracked sensitively by analytical balance. Chemical composition of material, reinforcement content, solvent amount of specimen and thermal stability can be analyzed from the analysis diagram based on the difference in decomposition temperature [90]. DSC results are generally confirmed and supported with TGA results to verify the chemical characteristics of the specimen.

Thermal analysis are performed by using Perkin Elmer, TGA 8000 equipment with 10°C/min ramp rate under nitrogen environment by heating specimen from room temperature until 700°C. Neat CNT BPs and CNT BP/LDPE core layers which are compressed with LDPE films and also melt mixed CNT/HDPE films are characterized by TGA to be able to discriminate the effect of CNT reinforcing and cryogenic temperature on thermal stability also to calculate the actual polymer amount between CNT bundles.

2.3.2 Morphological analysis

Scanning electron microscopy (SEM)

The working principle of scanning electron microscopy (SEM), shown in Figure 2.13, is based on focused beam which generates electrons having high energy to scan and characterize the surface. After high-energy electrons generated by the electron beam, these electrons pass through several electromagnetic lenses, and then interact with the surface of specimen inside the vacuum chamber. The interaction of electrons with the surface generates lower-energy electrons and these reflected electrons are detected by X-ray and secondary detectors. Following the collection of the reflected electrons, images depending on the energy level of electrons appear on the computer screen and the surface morphology in three dimensional form is evaluated in detail [91].

Morphological analyses of both CNT BP/LDPE core layers and CNT reinforced UHMWPE laminated composites are investigated by using Zeiss Sigma VP equipment for SEM imaging at different magnifications at Teijin Aramid. Due to SBS test requirements, composite dimensions are small enough to directly place specimens into the SEM chamber; therefore, no additional sample preparation step is performed. The state of the wetting and the adhesion of CNT BPs are analyzed by SEM images leading to optimize manufacturing processes.

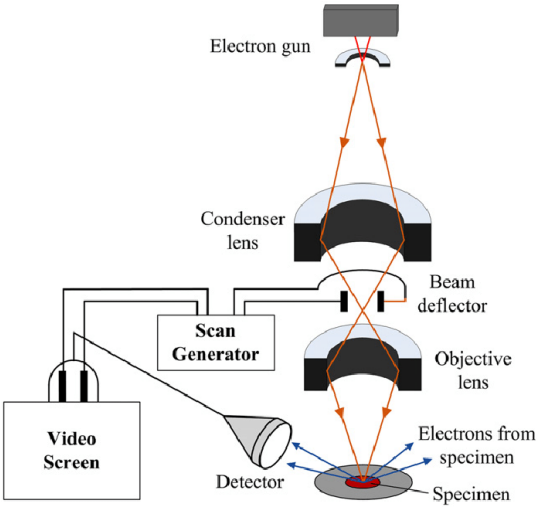

Figure 2.13: Working principle of SEM [92].

Morphological analysis with optical microscope

Optical microscope, also named as light microscope, is commonly used as visualization technique to scan the surface of materials. Visible light is used as a scanning source with various lenses for magnification in this microscope which also enables fast and practical analysis. Owing to allowing relatively colorful imaging and being easy-to-use, visual microscopes are preferable techniques instead of SEM or TEM if extreme magnifications are not required. Failure type of composites and failure location on composites are identified after SBS tests by optical microscope at different magnification at Teijin Aramid facility and Istanbul Technical University Aerospace Research Center (ITUARC).

CNT BP surface analysis by Brunauer–Emmett–Teller (BET) method

Brunauer, Emmett and Teller (BET) analysis is a surface analysis method for porous materials to figure out specific surface area, pore volume, porosity percentage also pore sizes and their distribution. The main working principle of BET analysis is to flow gas or vapor through the specimen and to measure the gas amount at the inlet and outlet of the sample in liquid nitrogen environment (-196˚C). The amount of adsorbed gas, which is generally nitrogen, by the specimen is in correlation with specific surface area. Relative pressure and nitrogen gas per mass of sample are measured to obtain specific surface area or porosity [93-95].

BET analysis is performed by using Micrometics 3 Flex BET Surface Analyzer Instrument at liquid nitrogen environment (-196˚C) with relative pressure (P/P_0) from 0.04 to 0.3 after degassing the specimens under vacuum.

Calculation of specific surface area (S) is done by using the Eqs. (2.1) and (2.2) [96];

$$\frac{1}{v[\left(\frac{P}{P_0}\right)-1]} = \frac{C-1}{V_m C}\left(\frac{P}{P_0}\right) + \frac{1}{V_m C} \tag{2.1}$$

$$S = \frac{V_m N A}{22.4\ x\ m} \tag{2.2}$$

where V is the adsorbed volume of gas, V_m is the adsorbed monolayer volume, C is the BET constant, N is the Avogadro's number, A is the cross-sectional surface area of a single adsorbed gas molecule and m is the mass of materials used in the measurements. The correlation between porosity and pore volume is established by Eqs. (2.3) and (2.4) [96];

$$V_{liq} = \frac{P_a\ V_{ads}\ V_m}{R\ T} \tag{2.3}$$

$$r_p = \frac{2\ V_{liq}}{S} \tag{2.4}$$

where V_{liq} is the volume of liquid N_2 in pores, V_{ads} is the volume of gas adsorbed, V_m is the molar volume of liquid adsorbate, P_a is the ambient pressure, T is the ambient temperature and r_p gives the porosity and pore radius relation.

2.3.3 Mechanical tests

2.3.3.1 Short beam shear tests at room temperature (20°C)

Short-beam shear **(**SBS) tests are performed in compliance with ASTM D2344 which states how to calculate ILSS under pure shear loading via 3-point bending test. In this setup, the distance between the supports is set to 24 mm, the depth of them is 16 mm and diameters of the loading roller and supports are 12 mm and 6 mm, respectively as seen in Figure 2.14. These dimensions are slightly different than the ASTM D2344 standard but they are based on the research which is conducted by Adams [97]. In the research, the change in failure type regarding to the thickness-to-span ratio and loading cylinder diameter is investigated on varied composite materials. At higher thickness-to-span ratios which are over than 9, pure bending failure is observed and also these bending test specimens are able to distribute stress along the length. Adams revealed that combined failure could be hindered by choosing

intermediate thickness-to-span ratios between 4 and 9, thus pure shear failure would be observed. Nevertheless, length of these specimens is not long enough to permit homogenous stress distribution along the specimen and through the thickness, which creates stress concentration regions. As an alternative solution, loading and support cylinders can be rearranged with larger diameter rollers different from the standard, which reduces the sensitivity of specimens against to change in span-to-thickness ratio and provides better stress distribution, consequently restrict local crushing. Based on this background, support and loading cylinders with larger diameters compared to the related standard are used in the test performing.

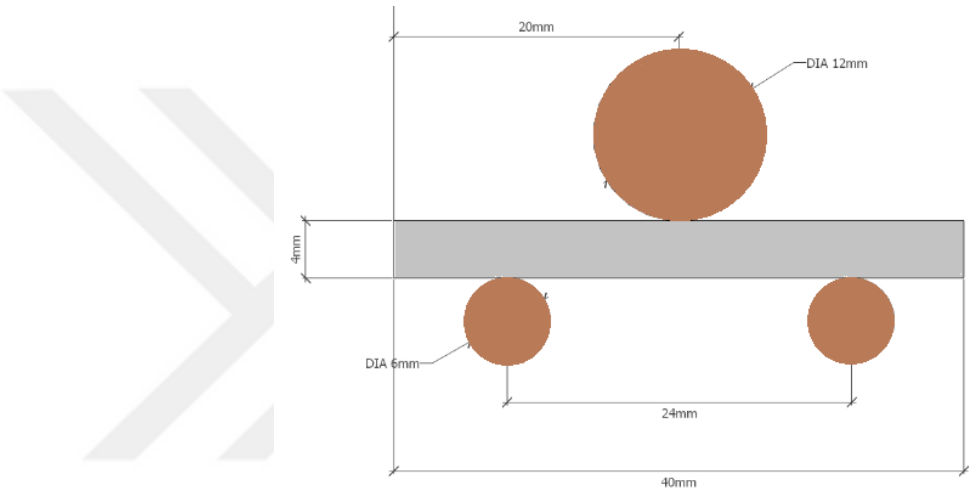

Figure 2.14: SBS test specimen, support, and load cylinder geometry.

During SBS tests, specimens are placed on two cylindrical supports as shown in Figure 2.15 and the other cylindrical head is moved in –z direction speed of 1.0 mm/min until significant bending is observed.

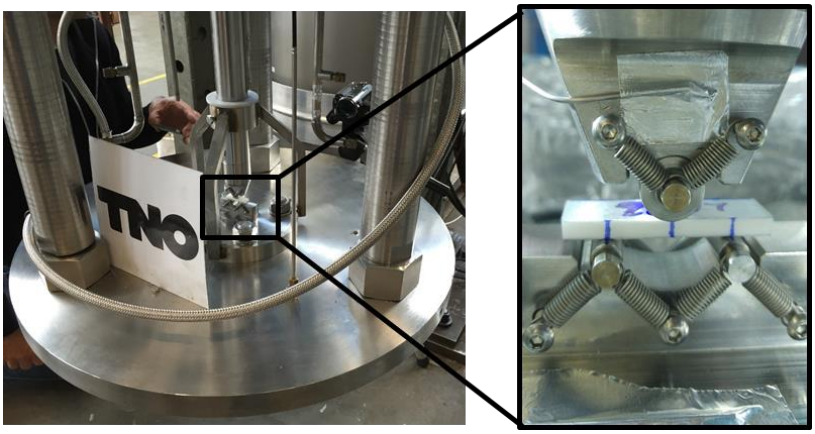

Figure 2.15: SBS test setup and assembly of specimen.

Force and displacement data which are recorded during testing and translated into ILSS by using Eq. (2.5) where F^{sbs} is the short-beam strength (MPa), P^m is the maximum load during tests (N), b is the width of specimen (mm) and h is the thickness of specimen (mm) as stated in the standard.

$$F^{sbs} = 0.75\ x\ \frac{P^m}{b\ x\ h} \tag{2.5}$$

2.3.1.2 Short beam shear (SBS) tests at liquid nitrogen (LN_2) temperature (-196°C)

The difference in ILSS characteristics of composites at different temperatures is evaluated by conducting tests in ambient air and liquid nitrogen (-196°C) environments. The uniaxial test setup is made of stainless steel and the insulation chamber is built from thick foam to create a pool of liquid nitrogen for specimens as shown in Figure 2.16.

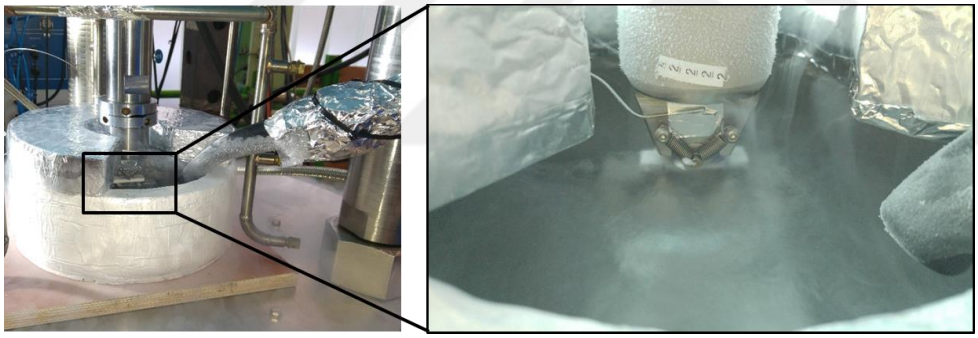

Figure 2.16: Insulation chamber for cryogenic tests at SBS test setup and assembly of specimen.

Temperature is controlled by K-type thermocouples which are placed on the top and bottom of the specimen to ensure that the temperature is stable prior to loading in the cryogenic tests. Data are recorded simultaneously during testing by data acquisition software (Figure 2.17).

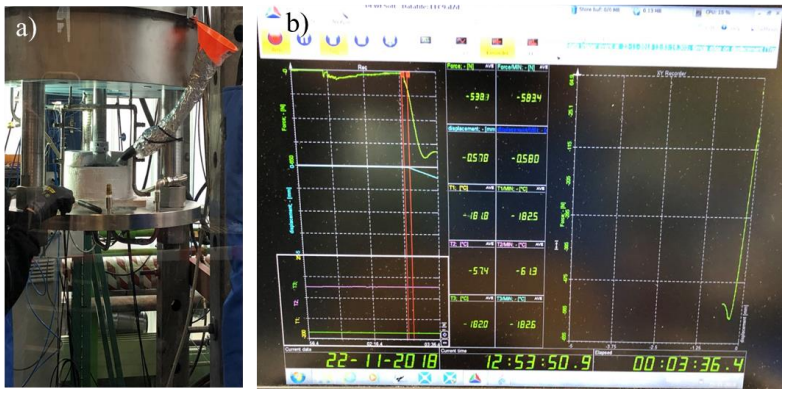

Figure 2.17: a) Cryogenic test setup, b) data acquisition system for temperature, force and displacement.

Results of SBS tests at room temperature show that the load carrying capability of laminated composites containing 0.13 and 0.2 wt.% CNT BPs, are relatively weaker which is attributed to less effective impregnation with polymer. Hence, the cryogenic tests for these laminated composites are not performed. Summary of performed tests is tabulated in Table 2.3.

Table 2.3: Summary of performed SBS tests.

Specimen Type	Room temperature SBS	Cryogenic SBS
Reference (Neat)	√	√
Melt mixed CNT/HDPE film	√	√
0.05 wt.% CNT BP	√	√
0.065 wt.% CNT BP	√	√
0.13 wt.% CNT BP	√	-
0.2 wt.% CNT BP	√	-

3. RESULTS AND DISCUSSIONS

3.1 Thermal Analysis of CNT Films and Composites

3.1.1 Differential scanning calorimetry (DSC)

Since mechanical properties of polymer composites are highly dominated by the crystalline structure of polymers, the correlation between these two terms is investigated for melt mixed CNT/HDPE film by performing DSC analysis. Considering DSC studies, the effects of cryogenic temperatures as well as CNT insertion on the crystalline structure of HDPE are studied.

In the case of DSC curves, which are illustrated in Figure 3.1, peak temperatures of neat HDPE and melt mixed CNT/HDPE films exposed to room and liquid nitrogen temperatures are 129.2 °C, 130.5 °C and 130.9 °C, respectively. As conformed by DSC results, peak temperature is not affected by integration of CNTs to composites and cryogenic conditions. Similar to peak temperature, onset temperature, which defines the propagation of crystalline sites of polymer, is slightly decreased with CNT addition. The reduction in crystallization temperature indicates increment of the crystallinity degree, which is attributed to the behavior of CNTs acting as nucleation sites within HDPE polymer chains.

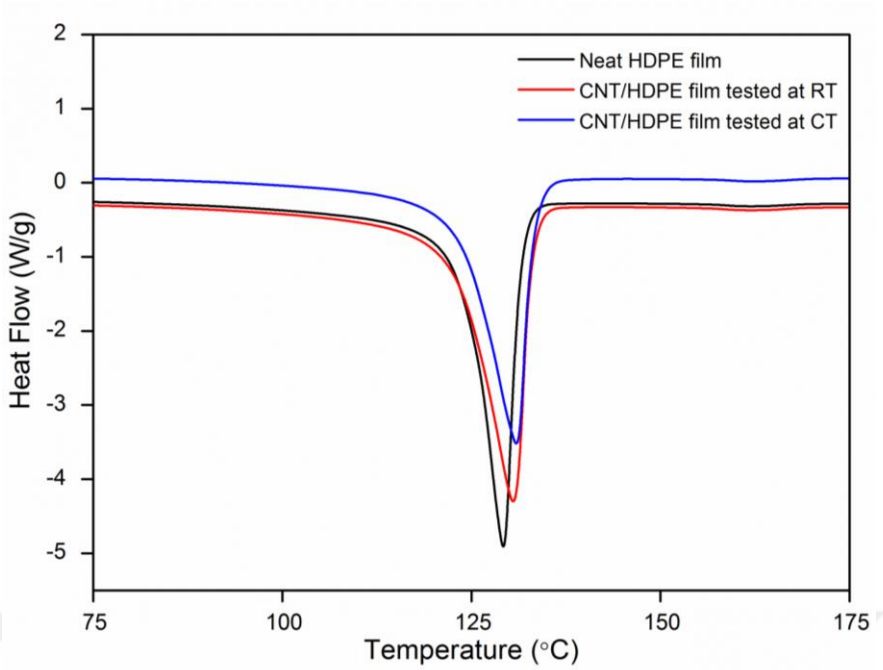

Figure 3.1: DSC curves of neat HDPE and CNT/HDPE films subjected to room and cryogenic temperatures.

The enthalpy of crystallization is 180.50 J/g, 191.62 J/g, and 169.66 J/g for neat HDPE, CNT/HDPE film tested at room temperature, and CNT/HDPE film subjected to liquid nitrogen during mechanical test, respectively. Besides peak and onset temperatures, the enthalpy of HDPE crystallization is increased due to the fast formation of crystalline structures within CNTs inclusion. Consequently, CNT insertion in the polymer structure allows liberating more energy during the crystallization. The percentage of crystalline site into the polymer which is crystallinity, X_c, is calculated depending on enthalpy values from the Eq. (3.1);

$$X_c = \frac{\Delta Hc}{(1-wt.\%)\,\Delta Hm}\ x\ 10 \qquad (3.1)$$

where ΔH_c is the heat evolved during crystallization, wt.% is the weight fraction of MWCNTs in the composites and ΔH_m is enthalpy of pure HDPE which is 293 J/g obtained from literature [34]. The calculated crystallinities are 61.6%, 81.75%, and 72.38% for neat HDPE, CNT/HDPE film tested at room temperature and CNT/HDPE film tested at cryogenic temperature, respectively. The enhanced crystallinity percentages of melt mixed CNT/HDPE films demonstrate the nucleating influence of CNTs through polymer chains, which improve the mechanical performance of polymer.

However, as presented in crystallinity percentages, cryogenic temperatures cause an appreciably decrease in the crystallinity of CNT/HDPE film compared to its counterpart in room temperature. At such extremely low temperatures, polymer chains shorten thereby more interface regions and defects are formed between polymer chains. As a result, this deteriorating effect of cryogenic temperatures on the formation of crystalline sites degrades the strength of composites compared with CNT/HDPE film reinforced composites tested at room temperature.

3.1.2 Thermogravimetric Analysis (TGA)

Thermal analysis of melt mixed CNT/HDPE films

CNT reinforcement as well as extreme change in environment temperature cause a variation in thermal properties of polymers. The effects of temperature and CNT inclusion on HDPE polymer are crucial to achieve accurate knowledge about the thermal behavior of composites and to prevent failure of cryogenic tanks due to thermal instabilities.

Figure 3.2 shows that neat HDPE exhibits same weight loss trend with the melt mixed CNT/HDPE films which are subjected to room and cryogenic temperatures during mechanical testing. However, above 400°C, the shift in thermal stability of HDPE to the higher temperatures with CNT reinforcement is attributed to the increase in the degree of cross linking, consequently crystallinity of HDPE as corresponded to DSC results. Moreover, in the case of melt mixed CNT/HDPE films, the minor change in thermal stability of film reveals that thermal stability is not much affected by exposing to extremely low temperature.

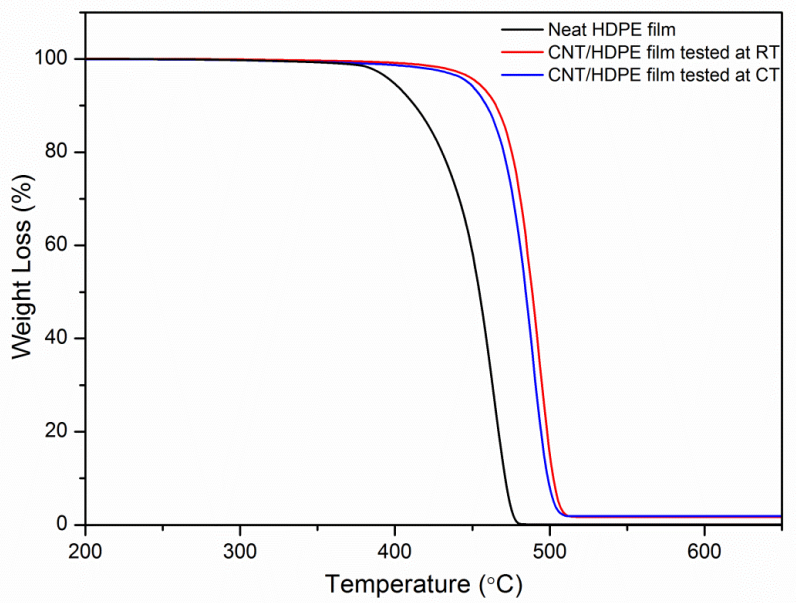

Figure 3.2: TGA thermograms of neat HDPE and CNT/HDPE films subjected to room and cryogenic temperatures.

The maximum decomposition temperatures are 464.2°C, 493.3°C, and 488.9°C as presented in Figure 3.3 for neat HDPE, melt mixed CNT/HDPE film subjected to room and cryogenic temperatures, respectively. Hence, the nucleation effects of CNTs within the HDPE and thermal stability enhancement by synergetic effects of CNTs are found in a correlation with DSC results.

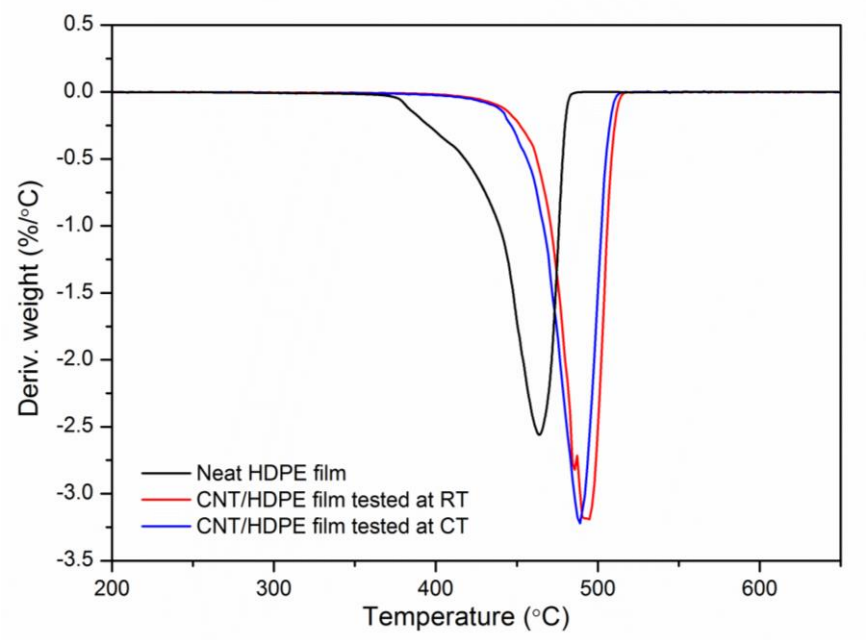

Figure 3.3: DTG curves of neat HDPE and melt mixed CNT/HDPE films subjected to room and cryogenic temperatures.

Thermal analysis of CNT BPs and CNT BP/LDPE films

Impregnation quality of CNT BP composites is evaluated quantitatively by calculating weight percentages of LDPE polymer into the composite structures to explore the efficiency of wetting process. Residue percentages of CNT BPs, LDPE films, and CNT BP/LDPE composites are obtained from TGA curves as shown in Figure 3.4 and Figure ***3.5***.

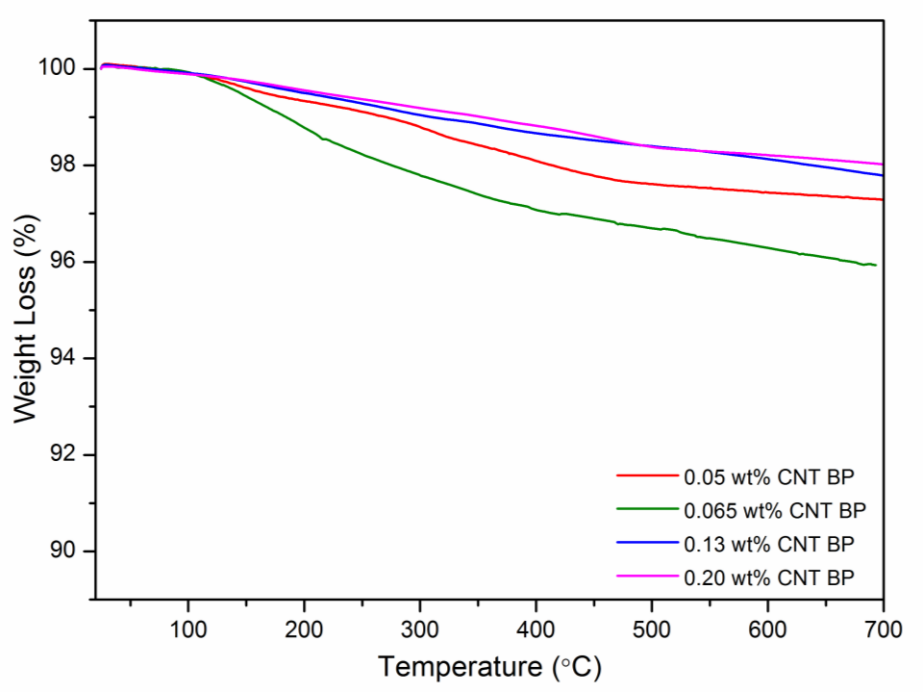

Figure 3.4: TGA curves of CNT BPs under nitrogen atmosphere.

As observed in Figure 3.4, residual percentages of CNTs within the BPs increases with incremental CNT weight fractions as expected. Only minimal deviation is noticed in residual percentages trend, which is at acceptable level among overall values. These values are represented as $R_{CNT\ BP}$ for different CNT BPs and tabulated in Table 3.1 for weight fraction calculations.

Table 3.1: Residual percentages of different CNT BPs.

	$R_{CNT\ BP}$
0.05 wt% CNT BP	97.06 %
0.065 wt% CNT BP	96.13%
0.13 wt% CNT BP	97.43 %
0.2 wt% CNT BP	97.77 %

Then, weight fraction of LDPE polymer in CNT BP core layers is calculated from following Eqs. (3.2) and (3.3);

$$W_{LDPE}.R_{LDPE} + W_{CNT\ BP}.R_{CNT\ BP} = R_{comp} \quad (3.2)$$

$$W_{CNT\ BP} + W_{LDPE} = 1 \quad (3.3)$$

where R_{LDPE} is residue percentage of LDPE; $W_{CNT\ BP}$ and W_{LDPE} are weight fractions of CNT BP and LDPE polymer within the core layers, respectively. Residual percentages of LDPE films and CNTs are obtained from TGA curves (see **Hata! Başvuru kaynağı bulunamadı.**) and listed in Table 3.2. Also, according to TGA measurements and mathematical calculations based on Eqs. (3.2) and (3.3), obtained weight percentages of LDPE and CNTs within the core layers are tabulated in Table 3.2.

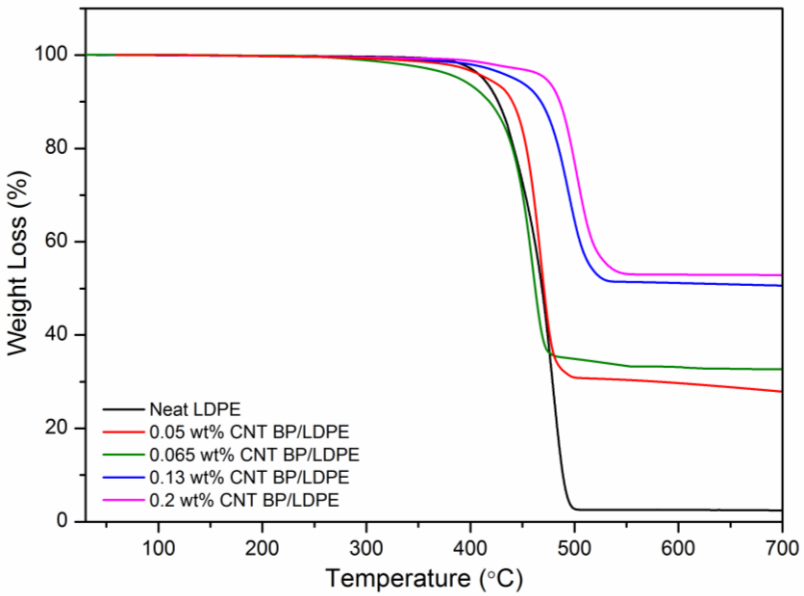

Figure 3.5: TGA thermograms of neat LDPE and CNT BP/LDPE composite samples.

Based on weight fractions of LDPE and CNTs within the core layers as listed in Table 3.2, it is concluded that LDPE progressively infuses through the vacancies between CNT bundles with decreasing CNT fractions. The replacement of vacancies with polymer is crucial to supply load transfer continuity through the CNT interlayer, which enhances strength of the composites. The improved ILSS performances of 0.05 and 0.065 wt.% CNT BP reinforced composites are proportional with the increasing weight fraction of LDPE providing a more efficient load transfer.

Table 3.2: Residual percentages and weight fractions of LDPE films and CNT BP/LDPE core layers.

	R_{LDPE}	R_{comp}	W_{LDPE}	$W_{CNT\ BP}$
Neat LDPE	1.94 %	-	-	-
0.05 wt% CNT BP/LDPE	-	26.2 %	0.745	0.255
0.065 wt% CNT BP/LDPE	-	32.5 %	0.676	0.324
0.13 wt% CNT BP/LDPE	-	50 %	0.497	0.503
0.2 wt% CNT BP/LDPE	-	52.7 %	0.471	0.529

Even though CNT BPs are impregnated into LDPE films, there could be still pores between CNT bundles. Discontinuities resulting from insufficient impregnation quality could degrade mechanical, electrical, and thermal properties of composites. Therefore, the calculation of volume fractions of LDPE polymer and pores into the composites is an essential procedure to figure out the correlation between bonding quality and mechanical performances of composites. Volume fractions of LDPE polymer and pores are calculated from the following (3.4) and (3.5) equations based on the research studied by Ashrafi *et al.* [98];

$$V_{LDPE} = \frac{\rho_{comp}.W_{LDPE}}{\rho_{LDPE}} \tag{3.4}$$

$$V_{pore} = 1 - V_{CNT\ BP} - V_{LDPE} = 1 - \frac{\rho_{comp}.W_{CNT\ BP}}{\rho_{CNT\ BP}} - \frac{\rho_{comp}.W_{LDPE}}{\rho_{LDPE}} \tag{3.5}$$

The difference between CNT BP theoretical density calculation approach based on Eq. (3.6) and stated values in literature is evaluated by calculating CNT and pore volume fractions from Eqs. (3.4) and (3.5). Based on the densities of CNTs and ethanol into the BP structure, densities of as-prepared CNT BPs are calculated according to the Eq. (3.6) and results are listed in the Table 3.3.

$$\frac{1}{\rho_{CNT\ BP}} = \frac{W_{CNT}}{\rho_{CNT}} + \frac{W_{ethanol}}{\rho_{ethanol}} \tag{3.6}$$

where $\rho_{CNT\ BP}$ is density of as-prepared CNT BP, ρ_{CNT} is density of CNT which is 2.1 g/cm^3, $\rho_{ethanol}$ is density of ethanol which is 0.79 g/cm^3, W_{CNT} and $W_{ethanol}$ are weight fractions of CNTs and ethanol obtained from TGA thermograms, respectively.

Table 3.3: Density values of as-prepared CNT BPs with different CNT weight fractions.

	W_{CNT}	$W_{ethanol}$	*$\rho_{CNT\ BP}$
0.05 wt.% CNT BP	0.971	0.029	2
0.065 wt.% CNT BP	0.961	0.039	1.97
0.13 wt.% CNT BP	0.974	0.026	2.01
0.2 wt.% CNT BP	0.977	0.023	2.03

*$\rho_{CNT\ BP}$ is experimental density value of as-prepared CNT BPs.

Volume fractions of LDPE polymer (V_{LDPE}) and pores (V_{pore}) into the BP composites are calculated according to Eqs. (3.4) and (3.5) and the results are listed in Table 3.4 to analytically utilize impregnation quality. These data provide supplementary information for BET surface analysis. Pore volume fraction significantly decreases with increasing CNT content. The major decrement in pore volume fraction indicates incompatible trend with mechanical test results. Therefore, the difference between theory and literature is evaluated by performing additional calculations.

Table 3.4: Densities of CNT BP/LDPE core layers and theoretical volume fractions of LDPE, CNTs and pores within the core layers.

	ρ_{comp}	V_{LPDE}	V_{CNT}	V_{pore}
0.05 wt.% CNT BP/LDPE	0.64	51.6	8.1	40.2
0.065 wt.% CNTBP/LDPE	0.69	50.5	11.3	38.2
0.13 wt.% CNT BP/LDPE	0.968	52.1	24.2	23.7
0.2 wt.% CNT BP/LDPE	1.232	62.8	32.1	5.1

As a complimentary approach, calculations are repeated with CNT BP density values based on the reported studies in the literature [98-100] different from the experimental results in this study. Density of as-prepared CNT BP is assumed as 0.55 g/cm^3 and 1.39 g/cm^3 for further volume fraction calculations and results are listed in Table 3.5.

Table 3.5: Volume fractions of CNTs and pores within the CNT BP/LDPE core layers based on density values of CNT BPs in literature.

	$*V_{LPDE}$	$*V_{CNT}$	$*V_{pore}$
0.05 wt.% CNT BP/LDPE	51.6	11.7	36.6
0.065 wt.% CNTBP/LDPE	50.5	16	33.4
0.13 wt.% CNT BP/LDPE	52.1	35	12.8
0.2 wt.% CNT BP/LDPE	62.8	46.8	-

*Calculations are performed according to 1.39 g/cm^3 for CNT BP density [99].

BPs with a higher CNT weight fraction tends to preserve more polymer within the bundles in which the vacaincies are replaced with CNTs governing a decrement in pore volume fraction. However, increase in CNT interlayer thickness overwhelms the synergetic effect of CNTs on mechanical performance of composites hence decrement in ILSS of 0.13 and 0.2 wt% CNT BP reinforced composites is observed.

Pore volume fractions with different CNT BP density values are compared by calculating different BP densities as shown in Figure 3.6. The range of fabricated CNT BPs densities in this study is varies from 1.97 to 2.03 with experimental approaches and these values are calculated according to Eq. (3.6). Owing to the fact that reported density values for high-density CNT BPs are in the 0.55 and 1.58 g/cm^3 range, experimental volume fraction calculations are varified with reported values. As a result of difference in fabrication processes of CNT BPs, thickness and eventually density vary for each type of process as reported in literature studies [98, 99]. Since same pore volume fraction trend is observed between experimental approach and literature, it is verified that coherent results with literature are obtained in this thesis.

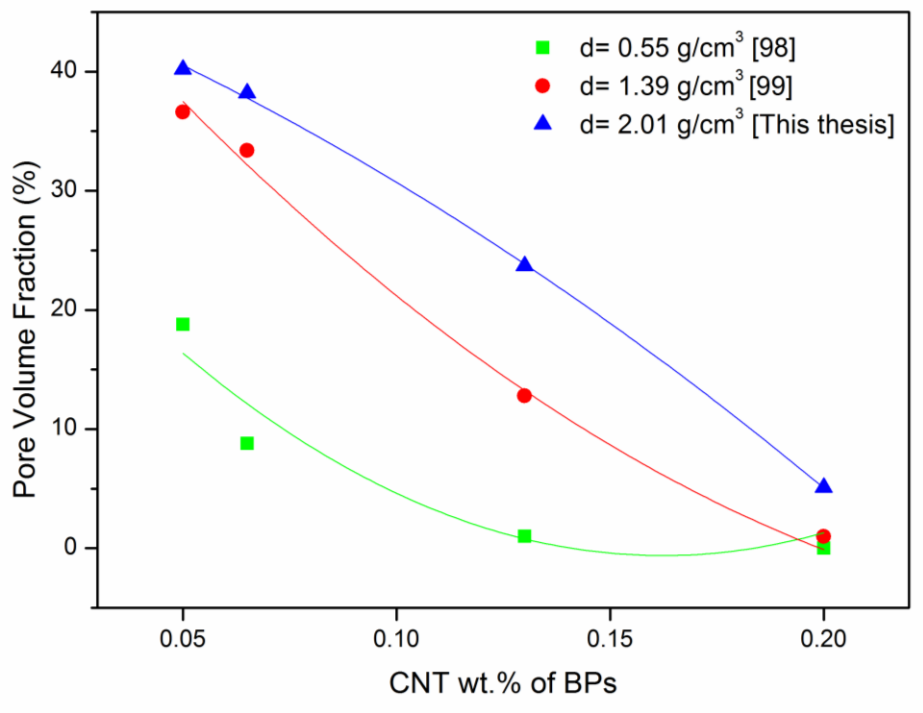

Figure 3.6: Pore volume fractions of CNT BPs with different CNT weight fractions and densities.

3.2 Morphological Analysis

After fabricating CNT BP and melt mixed CNT/HDPE film reinforced composites, their morphology is characterized by optical microscopy and SEM.

3.2.1 Morphological analysis with scanning electron microscopy (SEM) before mechanical tests

Morphology of CNT reinforced laminated composites are investigated through SEM images to identify the referring the bonding and impregnation quality of CNT interlayers with polymer. SEM micrographs of neat UHMWPE laminated composites without CNT interlayer is shown in Figure 3.7 wherein typical pathway of polymer fibrils resulting from water jet cutting are observed (see Figure 3.7b).

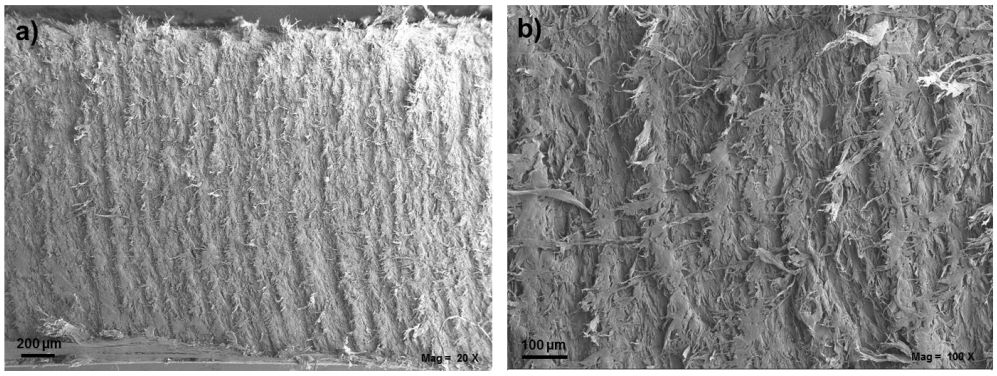

Figure 3.7: SEM images of neat UHMWPE laminated composite from the side view before SBS test.

The interface areas of 0.05 and 0.065 wt.% CNT BPs reinforced laminated composites between CNT BPs and UHMWPE films, as given in Figure 3.8, show uniform structure through the length of specimens without any bonding defects. Sufficiently wetted CNT BPs/LDPE indicates adequate load transfer through the structure. SEM images with high magnification (Figure 3.8c and Figure ***3.8***f) reveal the homogeneous dispersion of CNTs without any significant agglomerations and uniform impregnation of CNTs with LDPE through the composite. According to obtained inferences after SEM imaging and the reported studies on synergetic effects of thinner CNT interlayers on the mechanical properties of composites [101], it is concluded that 0.05 and 0.065 wt.% CNT BPs are promising reinforcements to be embedded in LDPE due to their low thickness.

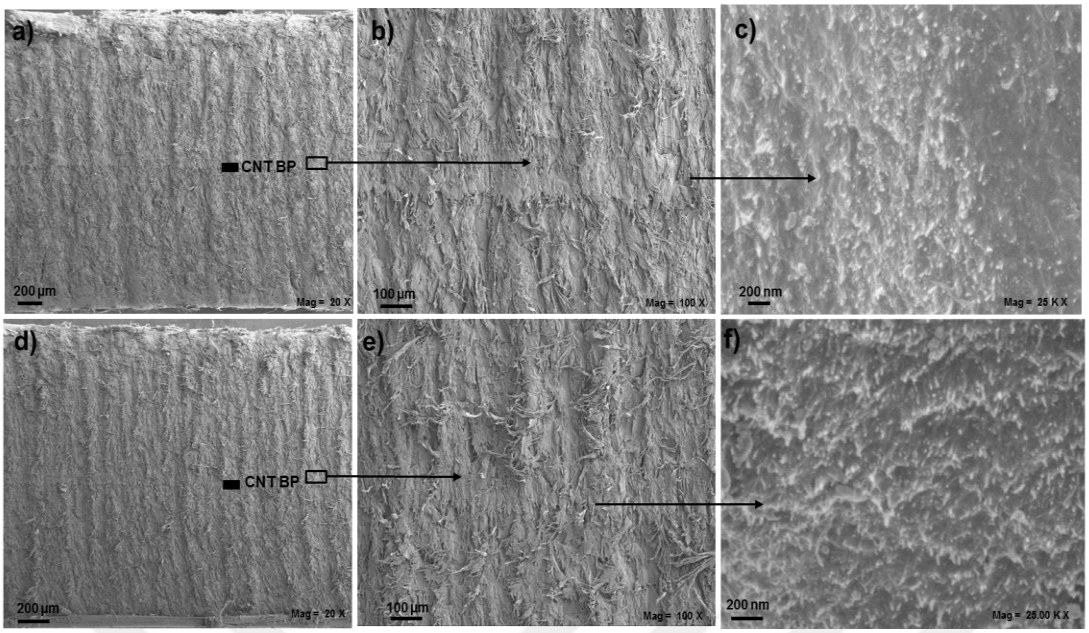

Figure 3.8: SEM images of; (a, b, c) 0.05 wt.% CNT BP and (d, e, f) 0.065 wt.% CNT BP reinforced UHMWPE laminated composites from the side view of composites before SBS test.

Increasing CNT weight fractions from 0.13 to 0.2 wt.%, consequently increasing CNT interlayer thickness alter the mechanical response of structure. Reinforced laminated composites with thicker BP interlayers including discontinuity regions through the interface exhibit an inadequate impregnation quality of CNT BPs with LDPE films in the composite thickness direction as observed in Figure 3.9b and Figure ***3.9***e. In addition to discontinuities, agglomerations of CNTs indicating the insufficient dispersion of CNTs into the BP are observed in Figure 3.9f. As a consequence of morphological observations from SEM images, it is envisioned that such imperfections through the composite thickness could degrade the mechanical properties of composites instead of enhancing the load carrying capability.

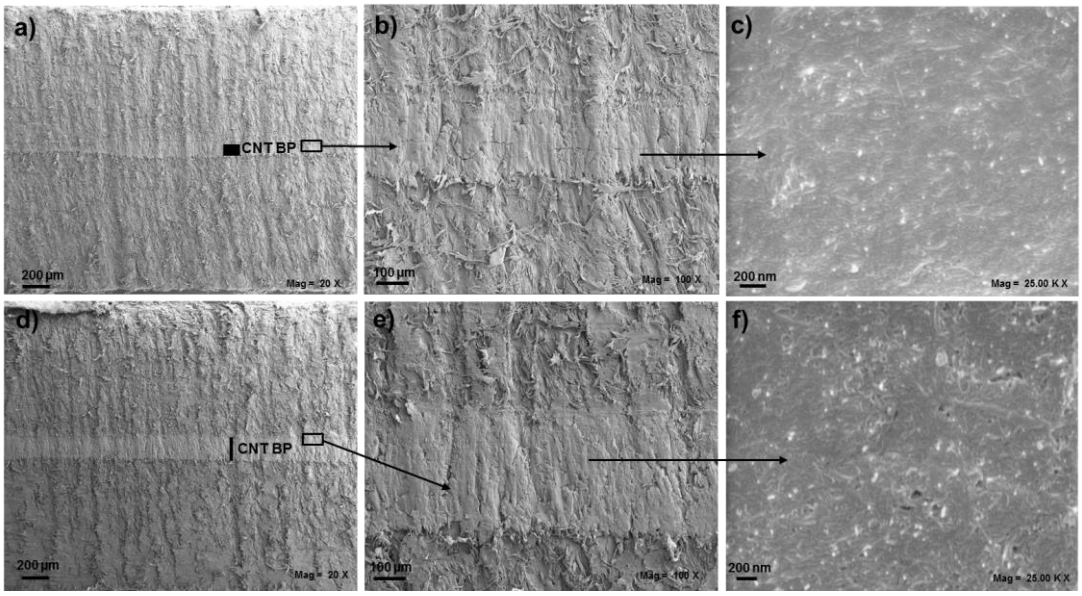

Figure 3.9: SEM images of; (a, b, c) 0.13 wt.% CNT BP and (d, e, f) 0.2 wt.% CNT BP reinforced UHMWPE laminated composites from the side view of composites before SBS test.

Besides the morphological analysis of CNT BP reinforced composites, melt mixed CNT/HDPE film reinforced composites are examined to compare adhesion quality with CNT BP reinforced composites. As seen in Figure 3.10a and Figure ***3.10***b, unlike thicker CNT BPs, discontinuities are not observed for melt mixed film, which is attributed to improved compatibility and adhesion between CNT interlayer and UHMWPE film. Even if there are small agglomerations observed in Figure 3.10c, there is still a homogenous distribution of CNTs in the HDPE matrix, which clarifies the enhanced interlaminar properties of reinforced composites.

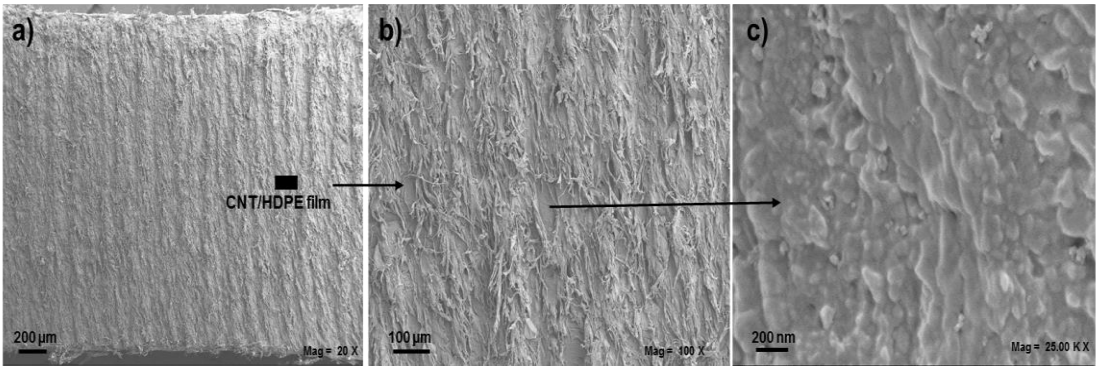

Figure 3.10: SEM images of melt mixed 0.2 wt.% CNT/HDPE film reinforced UHMWPE laminated composite from the side view before SBS test.

3.2.2 Morphological analysis with optical microscope

In order to identify the delamination characteristics of CNT BP and melt mixed CNT/HDPE film reinforced Endumax® composites, optical microscopic images are

assessed. Typical optical micrograph of 0.065 wt.% CNT BP reinforced Endumax® composite exhibiting interlaminar shear failure near the bottom surface at room temperature after SBS test is shown in Figure 3.11 as a representative image for 0.05 wt.% and 0.065 wt.% CNT BP and melt mixed CNT/HDPE film reinforced specimens. The optical microscopic examinations of the tested SBS specimens reveal that interlaminar shear failure occurs near the surfaces of the specimen indicating the strong bonding between the Endumax® films and CNT interlayer. The crack initiation region near the surface resulting from indentation of support rollers induces stress concentration areas and triggers delamination.

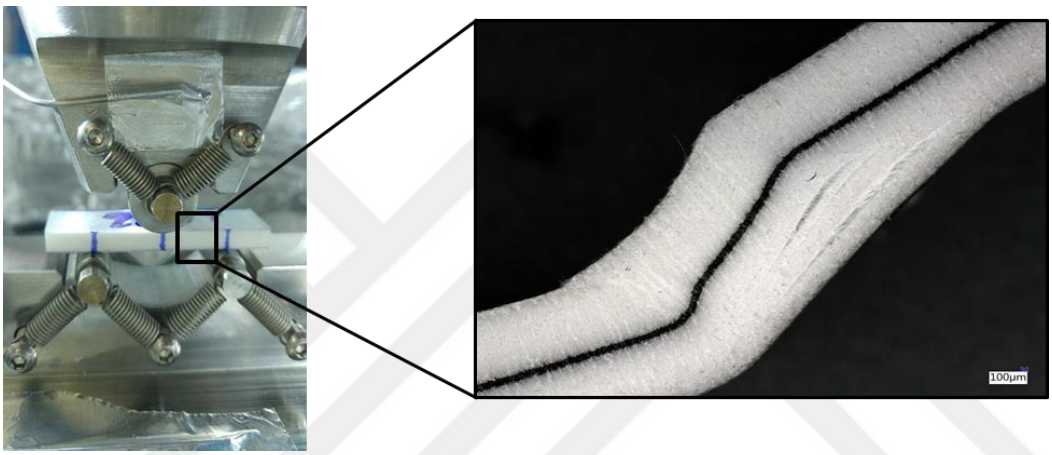

Figure 3.11: Representative image for 0.05 and 0.065 wt.% CNT BP and melt mixed CNT/HDPE reinforced composites after SBS tests at room temperature.

Contrarily, 0.13 wt.% and 0.2 wt.% CNT BP reinforced composites exhibit interlaminar shear failure at the CNT BP/Endumax® film interface as shown in Figure 3.12. The resulting adverse effect of thick CNT BP interlayers on the continuity of load transferring through the composite thickness induced different failure characteristic and delamination location. Microscopic inspection of *post mortem* specimens including thick CNT BPs reveals that thicker interface triggers delamination and weakens the interfacial area of composite, thereby diminishes the ILSS of structure.

Figure 3.12: Representative optical microscope image for 0.13 and 0.2 wt.% CNT BP reinforced composites after SBS tests at room temperature.

In addition to composites tested at room temperature, CNT BP and melt mixed CNT/HDPE film reinforced composites tested at liquid nitrogen temperature (77 K) are also investigated to clarify their failure mechanisms. Cryogenic tests are performed for 0.05 and 0.065 wt.% CNT BP which are the thinnest CNT BPs among CNT BPs in different weight percentages and melt mixed CNT/HDPE film reinforced UHMWPE laminated composites. As discerned in the representative microscopic image (Figure 3.13) for these three composites, any interlaminar failure through the mid plane is not recognized which implies the sufficient adhesion between CNT interlayer and UHMWPE films. These results further support the hypothesis that CNT interlayers strengthen the interfacial area of polymer plies within the composite, thus delamination does not occur through the CNT/polymer interface consequently structures could endure the higher load limit at cryogenic temperature.

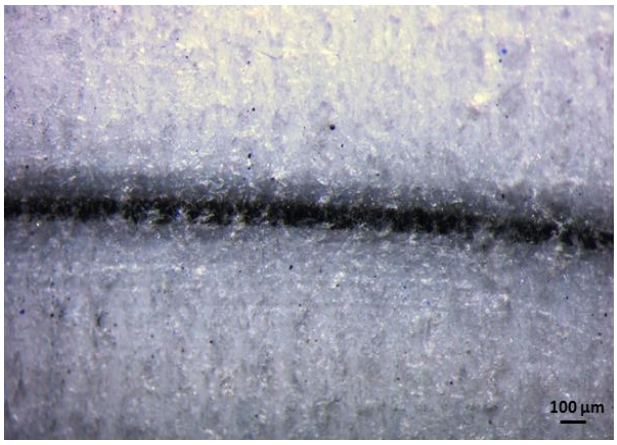

Figure 3.13: Typical failure image after SBS tests at cryogenic temperature for 0.05, 0.065 wt.% CNT BP and melt mixed CNT/HDPE film reinforced composites.

3.2.3 Morphological analysis with Brunauer, Emmett and Teller (BET) analysis

Impregnation quality of CNT/LDPE core layers is evaluated by conducting BET surface analysis. Specific surface area (SSA) and pore size clarify the occupation of vacancies between CNT bundles with polymer which yields into a more efficient load transfer between composite laminates. BET analysis results of 0.05 and 0.065 wt.% CNT BP/LDPE core layers are tabulated in the Table 3.6 exhibiting outstanding mechanical performance at room temperature. Average pore sizes of core layers increase at higher CNT content with constant LDPE amount, which increases the porosity of BPs. Same amount of LDPE exceptionally fills pores within 0.05 wt.% CNT BP as deduced from lower SSA of CNT BP than 0.065 wt.% CNT BP (see Table 3.6). The decrement in ILSS of 0.065 wt% CNT BP reinforced composite is attributed to the increment in porosity when compared to 0.05 wt% CNT BP reinforced composite.

Table 3.6: Specific surface area (SSA) and average pore size of CNT BP/LDPE core layers according to BET analysis.

	SSA(m^2/g)	***Pore size (nm)***
0.05 wt% CNT BP/LDPE	33	22.2
0.065 wt% CNT BP/LDPE	35.8	31.2

3.3 Mechanical Test Results of Composites

Mechanical tests are performed at both room and cryogenic temperatures to fully understand the effect of change in thermal properties of composites on mechanical properties of composites with CNT inclusion and exposure to cryogenic temperatures.

3.3.1 Room temperature short beam shear (SBS) test results

The representative room temperature load-displacement curves of neat laminates, UHMWPE composites reinforced with 0.05 wt.% CNT BP, 0.065 wt.% CNT BP, 0.13 wt.% CNT BP, 0.2 wt.% CNT BP, and melt mixed 0.2 wt.% CNT/HDPE film are exhibited in Figure 3.14. The failure mechanisms of all composites except melt mixed film reinforced composites proceed in three main steps. At first, the load proportionally changes with displacement followed by the decrease in load due to

indentation as a plastic failure resulting from support noses. In the end, a sudden drop is clearly observed after the specific deformation (2.5 mm). As reported in scientific researches [102, 103], the complex stress distribution on composite laminates during SBS tests lead to combined failure mechanism such as indentation, microcracking and interlaminar shear. Referring to the different failure modes in the standard [86], herein, failures are dominated by interlaminar damages. Following the first decline (less than 30% of the maximum load) in load-displacement curve corresponding to crushing of laminates, the maximum load defines the strength of composite [103]. Melt mixed CNT/HDPE film reinforced composites maintain the load carrying even beyond the critical deformation limit (2.5 mm) compared to 0.05 wt.% CNT BP which has similar nano-layer thickness. The enhancement in load carrying capability of melt mixed CNT/HDPE film is related to HDPE polymer as a base material, which provides compatibility between the core layer and HDPE side of Endumax® for the interface. Furthermore, more uniform dispersion of CNTs within HDPE contributes effective load transferring and prevents the formation of stress concentration regions. The main principle of CNT reinforcing strategy is based on increasing the load carrying capability of composite and delaying crack propagation by crack bridging effect [104]. The load-displacement curve of the highest weight percentage and eventually thickest (0.2 wt.%) CNT BP reinforced composites rises, flattens for some time and then shows a sudden drop at a specific displacement value (0.7 mm) after the crack initiation whereas other specimens show more stable behavior. Hence, thicker CNT interface causes weak load transfer between composite laminates, consequently triggers delamination through the laminates. Furthermore, CNT agglomerations observed in SEM images of 0.13 and 0.2 wt.% BPs (see Figure 3.9c and Figure ***3.9***f) induce stress concentration regions and weaken the CNT-polymer interface, which leads to a decrement in composite strength. In contrast, thinner CNT BPs which have 0.05 and 0.065 wt.% CNT content, show identical characteristics with the neat composite till the end of the test. The first drop in load-displacement graph results from composites indentation owing to stress concentrations arising from supports, yet specimen continues to still carry the load.

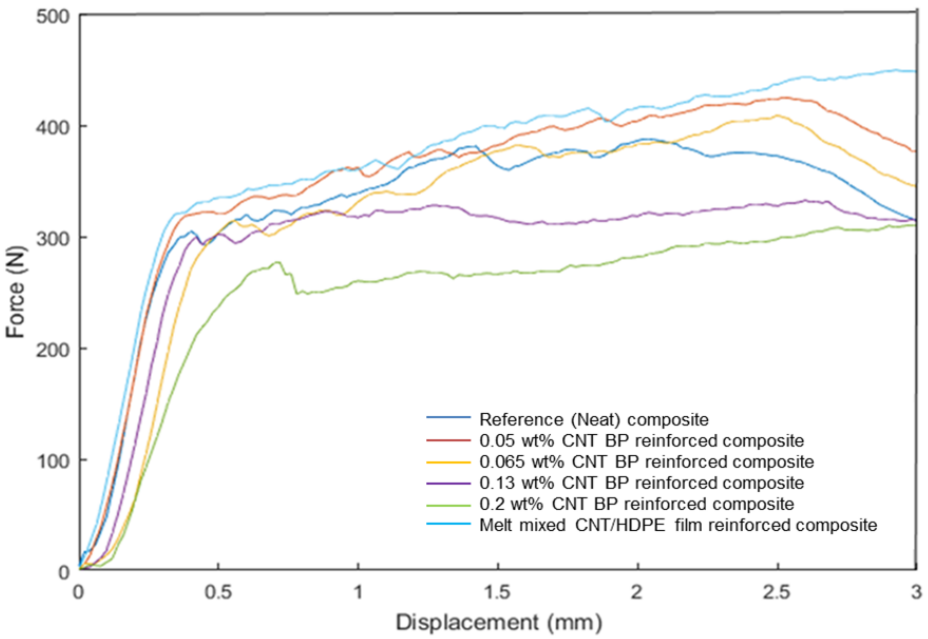

Figure 3.14: Force-displacement curves for SBS tests at room temperature.

Furthermore, since neat and laminated composites reinforced with melt mixed film, 0.05 wt.% CNT BP, and 0.065 wt.% CNT BP present best performance by considering the load-displacement curve, ILSS values are calculated for these composite configurations. The ILSS values of the specimens are displayed in Figure 3.15 and the reinforced composites with melt mixed CNT/HDPE film, 0.05 wt.% CNT BP, and 0.065 wt.% CNT BP present enhancements of 13%, 9.5% and 6.4% in ILSS values, respectively compared to the neat UHMWPE composite at room temperature.

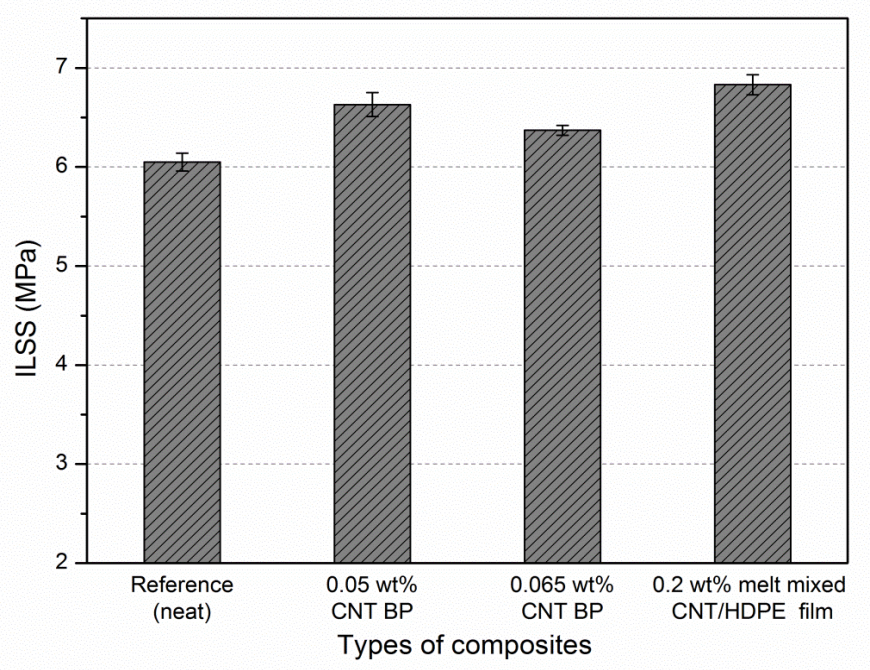

Figure 3.15: ILSS values of composites according to SBS test results at room temperature.

3.3.2 Liquid nitrogen temperature short beam shear (SBS) test results

To simulate the cryogenic conditions during operations of cryogenic substances, SBS tests are performed in the chamber filled with liquid nitrogen and specimens are exposed to extremely low temperature. When the force-deflection curves of all samples tested at room temperature are plotted, the results show that two specimen configurations which are reinforced with thick CNT BPs having 0.13 and 0.2 wt.% CNTs exhibit weaker load carrying performances than the neat laminates. Therefore, SBS tests are performed in liquid nitrogen environment with all composite types except 0.13 and 0.2 wt.% CNT BPs laminate configurations. As reported by the UHMWPE film manufacturer [78], Endumax® films become stronger at 77 K than the room temperature on the contrary to other high-performance materials. The maximum load carried by the composites considerably increases at low temperature conforming to supplier report. As clearly observed in Figure 3.16, the behavior of the all tested specimens changes from elastic to relatively brittle characteristic under loading compared to composites tested at room temperature, which is owing to the restriction of closer polymer chains at certain low temperature [15]. All samples tested at cryogenic temperature exhibit similar predominant interlaminar shear failure occurred near the bottom surface in comparison to the specimens tested at room

temperature and indicate sufficient adhesion between CNT core layer and UHMWPE films.

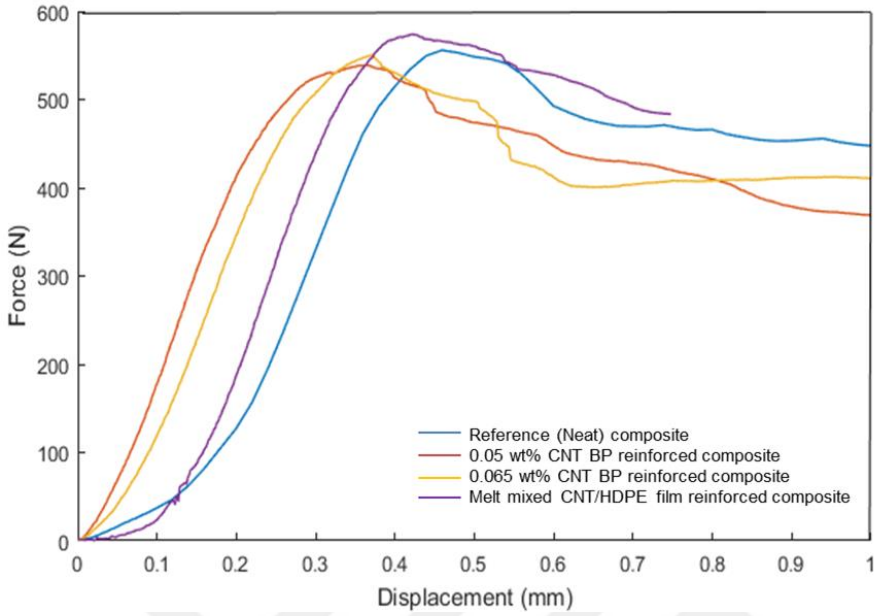

Figure 3.16: Force-displacement curves for SBS tests at cryogenic temperature.

0.05 wt.% CNT BP is the lowest ILSS among three reinforcement types while melt mixed CNT/HDPE film still shows the best mechanical performance. The achieved ILSS enhancement is 3.2% for the melt mixed CNT/HDPE film reinforced sample (see Figure 3.17). Within the CNT core layer reinforced specimens, no statistically significant change in ILSS is observed after CNT interlayer integration. The decrement in ILSS improvement of melt mixed CNT/HDPE film reinforced composites results from the degradation of crystalline sites in HDPE chains due to the cryogenic temperature, which is proved by DSC analysis. However, the difference in thermal expansion coefficients of CNT and polymer laminates induces thermal residual stress which predominantly affects the mechanical performance of composites. The deteriorating effect of the CNT BP overwhelms the reinforcing effect for efficient load transfer resulting in a decrease in ILSS of 0.05 wt.% and 0.065 wt.% CNT BP reinforced composites. Hence, the interfacial adhesion between the laminates would be weakened by the insertion of CNT BPs having 0.05 and 0.065 wt.% CNT contents.

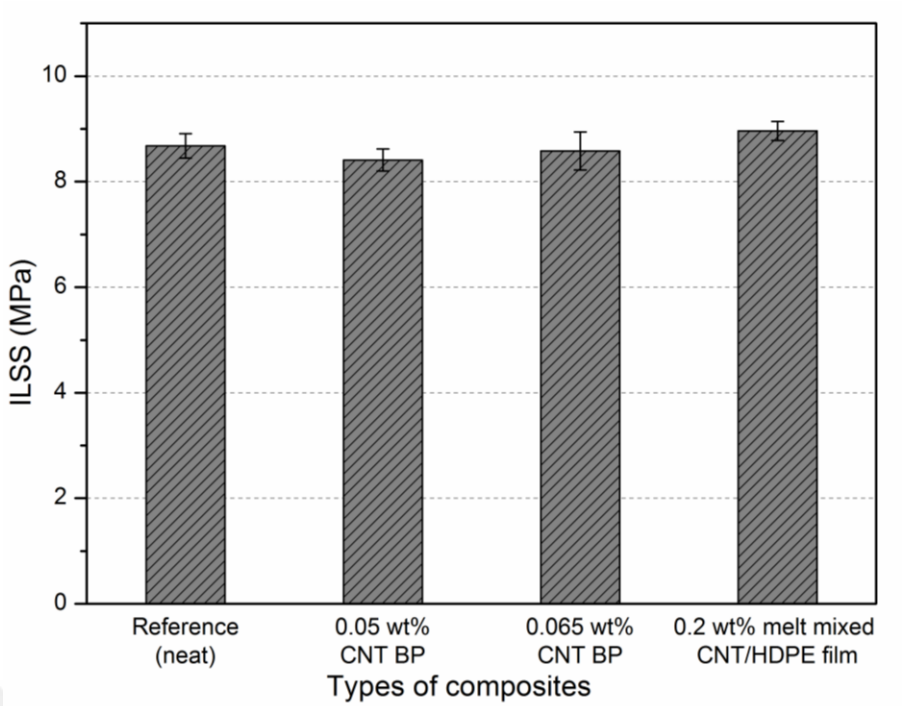

Figure 3.17: ILSS values of composites according to SBS test results at cryogenic temperature.

4. CONCLUSION

The effect of interlayered CNT reinforcement on mechanical performance of UHMWPE laminated composites are studied through SBS test under extreme condition which is liquid nitrogen (77 K) temperature relevant with LNG storage conditions. Within the scope of this research, two distinct CNT interleaving forms which are buckypaper form and melt mixed CNT/HDPE film are stacked in the mid-plane of UHMWPE laminates where maximum shear loading occurs during mechanical test. The thickness of core layer precisely alters load transfer mechanism through the composite thickness, which plays major role in mechanical performance of composite. CNT BPs in different weight fractions are fabricated by ultrasound sonication technique and CNT BPs with variable thicknesses are obtained. In case of melt mixed CNT/HDPE film reinforcement, CNT/HDPE granules are compressed to form thin film following the extrusion process in twin-screw extruder. The ILSS of laminated composite in diverse reinforcing configurations is evaluated via SBS tests performed at both room and cryogenic temperatures. Melt mixed CNT/HDPE film is found as an effective reinforcement for interlaminar strengthening and ILSS shows 13% enhancement at room temperature and 3% at cryogenic temperature over neat UHMWPE laminated composite. Besides melt mixed CNT/HDPE film, CNT BPs having 0.05 and 0.065 wt.% CNTs improves ILSS of UHMWPE composite at room temperature by 9.5% and 6.4%, respectively. Morphological characterizations reveal that melt mixed film and thin CNT BPs show superior adhesion quality with UHMWPE films as seen in SEM images compared to thick CNT BPs. In these SEM images, CNT agglomerations and stress concentration regions arising from weak CNT-polymer interface reveal the decrement of ILSS of composites. The correlation between thermal and mechanical properties of composites is established by performing thermal characterizations of CNT BPs as well as melt mixed CNT/HDPE film. Furthermore, the impregnation quality of CNT BPs is calculated analytically from TGA thermographs and the results demonstrate that 0.05 and 0.065 wt% CNT BPs show prominent impregnation, which is highly correlated with higher ILSS values of stated CNT BPs reinforced composites. To identify the changes originated from extremely low temperature and CNT inclusion on the crystallinity and thermal

stability of polymer, melt mixed CNT/HDPE film is characterized through DSC and TGA as complementary studies. According to DSC results, crystallinities of neat HDPE and CNT reinforced HDPE before and after cryogenic temperatures are calculated. Thus, it is concluded that while CNT inclusion increases the crystallinity of the polymer, cryogenic temperatures degrade crystalline sites within the polymer, which clarifies the decrement in ILSS improvement at cryogenic temperature compared to room temperature. Results from this work promote to identify the correlation between thermal and mechanical characteristics of thermoplastic composites reinforced with CNTs by distinctive strategies at extreme environments.

REFERENCES

[1] **Biron, M.**, *Thermoplastics and Thermoplastic Composites*. 2013, William Andrew.

[2] **Chavan, A**. *The Plastic Wars: Difference Between Thermoplastics and Thermosets*. 2018; Available from: https://sciencestruck.com/difference-between-thermoplastics-thermosets.

[3] **Mastro, P.F.**, *Plastics Product Design*. 2016: John Wiley & Sons Inc.

[4] **Group, S.** *Thermoplastic Composite Materials Applications*. Available from: https://www.sglgroup.com/cms/international/products/product-groups/cm/thermoplastic-composite-materials/industry.html?__locale=en.

[5] **Chemistry, A.I.** *Thermoplastic composites and advanced composites with outstanding properties*. Available from: https://www.arkema.com/en/innovation/lightweight-materials-and-design/thermoplastic-composites/.

[6] **Jay, M.L.**, *Thermoplastic Composites Featured in New Research and Applications*, in *Composites Manufacturing Magazine*. 2018.

[7] **Lin, J.H., et al.**, *Research on Processing Technology of Polyester Fabric Reinforced Polypropylene Thermoplastic Laminated Composites.* Advanced Materials Research, 2011. **284-286**: p. 373-376.

[8] **Kuo, M.C., et al.**, *Fabrication of High Performance Magnesium/Carbon-Fiber/PEEK Laminated Composites.* Materials Transactions, 2003. **44**(8).

[9] **Zheng, H., et al.**, *The Application of Carbon Fiber Composites in Cryotank.* 2018.

[10] **Johnson, T.F., D.W. Sleight, and R.A. Martin**, *Structures and Design Phase I Summary For The Nasa Composite Cryotank Technology Demonstration Project*, in *AIAA Science and Technology Forum*. 2013.

[11] **Johnson, T.F., D.W. Sleight, and R.A. Martin**, *Structures and Design Phase I Summary for the NASA Composite Cryotank Technology Demonstration Project.* 2013.

[12] **Kim, M.-G., J.-B. Moon, and C.-G. Kim**, *Effect of CNT functionalization on crack resistance of a carbon/epoxy composite at a cryogenic temperature.* Composites Part A: Applied Science and Manufacturing, 2012. **43**(9): p. 1620-1627.

[13] **Capiati, N.J. and R.S. Porter**, *The concept of one polymer composites modelled with high density polyethylene*. JOURNAL OF MATERIALS SCIENCE, 1975. **10**: p. 1671-1677.

[14] **Karger-Kocsis, J. and T. Bárány**, *Single-polymer composites (SPCs): Status and future trends.* Composites Science and Technology, 2014. **92**: p. 77-94.

[15] **Liu, H., H. Ji, and X. Wang**, *Tribological properties of ultra-high molecular weight polyethylene at ultra-low temperature*. Cryogenics, 2013. **58**: p. 1-4.

[16] **Soleimani, N., et al.**, *Mechanical properties of nanoclay reinforced polypropylene composites at cryogenic temperature.* Journal of Reinforced Plastics and Composites, 2012. **31**(14): p. 967-976.

[17] **Wei, Z., et al.**, *Flexural fatigue performance and electrical resistance response of carbon nanotube-based polymer composites at cryogenic temperatures.* Cryogenics, 2014. **59**: p. 44-48.

[18] **Mittal, G., et al.**, *Reinforcements in multi-scale polymer composites: Processing, properties, and applications.* Composites Part B: Engineering, 2018. **138**: p. 122-139.

[19] **Hussein, A., et al.**, *Cryogenic fracture behavior of epoxy reinforced by a novel graphene oxide/poly(p -phenylenediamine) hybrid.* Composites Part B: Engineering, 2017. **129**: p. 133-142.

[20] **Shen, X.-J., et al.**, *Improved cryogenic interlaminar shear strength of glass fabric/epoxy composites by graphene oxide.* Composites Part B: Engineering, 2015. **73**: p. 126-131.
[21] **AzoNano**. *Silicon Dioxide, Silica (SiO2) Nanoparticles – Properties, Applications*. 2013; Available from: https://www.azonano.com/article.aspx?ArticleID=3398.
[22] **Iijima, S.**, *Carbon nanotubes: past, present, and future.* Physica B: Condensed Matter, 2002. **323**(1-4): p. 1-5.
[23] **Martins-Junior, P.A., et al.**, *Carbon nanotubes: directions and perspectives in oral regenerative medicine.* J Dent Res, 2013. **92**(7): p. 575-83.
[24] **Liu, L., W. Ma, and Z. Zhang**, *Macroscopic carbon nanotube assemblies: preparation, properties, and potential applications.* Small, 2011. **7**(11): p. 1504-20.
[25] **Haldorai, Y. and J.-J. Shim**, *Manufacturing Polymer Nanocomposites*, ed. S. Thomas, R. Muller, and J. Abraham. 2016: John Wiley & Sons, Inc.
[26] **Hussain, F., et al.**, *Review article: Polymer-matrix Nanocomposites, Processing, Manufacturing, and Application: An Overview.* Journal of Composite Materials, 2006. **40**(17): p. 1511-1575.
[27] **Saeed, K. and S.-Y. Park**, *Preparation and properties of multiwalled carbon nanotube/polycaprolactone nanocomposites.* Journal of Applied Polymer Science, 2007. **104**(3): p. 1957-1963.
[28] **Liang, J., et al.**, *Molecular-Level Dispersion of Graphene into Poly(vinyl alcohol) and Effective Reinforcement of their Nanocomposites.* Advanced Functional Materials, 2009. **19**(14): p. 2297-2302.
[29] **Ajayan, P.M., et al.**, *Aligned Carbon Nanotube Arrays Formed by Cutting a Polymer Resin-Nanotube Composite.* Science, 1994. **265**: p. 1212-1214.
[30] **Jin, L., C. Bower, and O. Zhou**, *Alignment of carbon nanotubes in a polymer matrix by mechanical stretching.* Applied Physics Letters, 1998. **73**(9): p. 1197-1199.
[31] **Tang, W., M.H. Santare, and S.G. Advani**, *Melt processing and mechanical property characterization of CNT-HDPE.* Carbon, 2003. **41**: p. 2779-2785.
[32] **PTFE-Machinery**. *Polymer Screw Extrusion*. 2019; Available from: http://ptfe-machinery.com/polymer-screw-extrusion/.
[33] **Socher, R., et al.**, *The influence of matrix viscosity on MWCNT dispersion and electrical properties in different thermoplastic nanocomposites.* Polymer, 2012. **53**(2): p. 495-504.
[34] **Ferreira, F.V., et al.**, *Influence of carbon nanotube concentration and sonication temperature on mechanical properties of HDPE CNT nanocomposites.* Fullerenes, Nanotubes and Carbon Nanostructures, 2017. **25**(9): p. 531-539.
[35] **Mahfuz, H.**, *Manufacturing and Characterization of Carbon Nanotube/Polyethylene Composites.* International Journal of Nanoscience, 2005. **4**(1): p. 55-72.
[36] **Shofner, M.L., V.N. Khabashesku, and E.V. Barrera**, *Processing and Mechanical Properties of Fluorinated Single-Wall Carbon Nanotube Polyethylene Composites.* Chemical Materials, 2006. **18**: p. 906-913.
[37] **McNally, T., et al.**, *Polyethylene multiwalled carbon nanotube composites.* Polymer, 2005. **46**(19): p. 8222-8232.
[38] **Bhattacharyya, A.R., et al.**, *Crystallization and orientation studies in polypropylene/single wall carbon nanotube composite.* Polymer, 2003. **44**(8): p. 2373-2377.
[39] **Koide, R.M., G.v.Z.d. França, and M.A. Luersen**, *An ant colony algorithm applied to lay-up optimization of laminated composite plates.* Latin American Journal of Solids and Structures, 2012. **10**: p. 491-504.
[40] **Stevanovic, D.**, *Mode I and mode II delamination properties of glass/vinyl-ester composite toughened by particulate modified interlayers.* Composites Science and Technology, 2003. **63**(13): p. 1949-1964.
[41] **White, K.L. and H.-J. Sue**, *Delamination toughness of fiber-reinforced composites containing a carbon nanotube/polyamide-12 epoxy thin film interlayer.* Polymer, 2012. **53**(1): p. 37-42.

[42] **Wong, D.W.Y., et al.**, *Interlaminar toughening of woven fabric carbon/epoxy composite laminates using hybrid aramid/phenoxy interleaves.* Composites Part A: Applied Science and Manufacturing, 2017. **101**: p. 151-159.
[43] **Crane, R.M. and E.T. Camponeschi**, *Experimental and Analytical Characterization of Multidimensionally Braided Graphite/Epoxy Composites.* Experimental Mechanics, 1986.
[44] **Garcia, E., et al.**, *Fabrication and multifunctional properties of a hybrid laminate with aligned carbon nanotubes grown In Situ.* Composites Science and Technology, 2008. **68**(9): p. 2034-2041.
[45] **Li, R., et al.**, *Hierarchical carbon nanotube carbon fiber unidirectional composites with preserved tensile and interfacial properties.* Composites Science and Technology, 2015. **117**: p. 139-145.
[46] **Wicks, S.S., R.G. de Villoria, and B.L. Wardle**, *Interlaminar and intralaminar reinforcement of composite laminates with aligned carbon nanotubes.* Composites Science and Technology, 2010. **70**(1): p. 20-28.
[47] **Downs, W.B. and R.T.K. Baker**, *Modification of the surface properties of carbon fibers via the catalytic growth of the carbon nanofiber.* Journal of Materials Research, 1995. **10**(3): p. 625-633.
[48] **Veedu, V.P., et al.**, *Multifunctional composites using reinforced laminae with carbon-nanotube forests.* Nat Mater, 2006. **5**(6): p. 457-62.
[49] **Garcia, E.J., B.L. Wardle, and A. John Hart**, *Joining prepreg composite interfaces with aligned carbon nanotubes.* Composites Part A: Applied Science and Manufacturing, 2008. **39**(6): p. 1065-1070.
[50] **Abot, J.L. and S. Yi**, *On the mechanical response of carbon nanotube array laminated composite materials.* Journal of Reinforced Plastics and Composites, 2010. **29**(22): p. 3401-3410.
[51] **Han, J.-H., et al.**, *CNT buckypaper/thermoplastic polyurethane composites with enhanced stiffness, strength and toughness.* Composites Science and Technology, 2014. **103**: p. 63-71.
[52] **Liu, L., J. Wu, and Y. Zhou**, *Enhanced delamination initiation stress and monitoring sensitivity of quasi-isotropic laminates under in-plane tension by interleaving with CNT buckypaper.* Composites Part A: Applied Science and Manufacturing, 2016. **89**: p. 10-17.
[53] **Li, Z., J.G. Park, and Z. Liang**, *High-Performance Multifunctional Thermoplastic Composites Enhanced by Aligned Buckypaper* Advanced Engineering Materials, 2016. **18**(8): p. 1460-1468.
[54] **Liu, L., L. Shen, and Y. Zhou**, *Improving the interlaminar fracture toughness of carbon/epoxy laminates by directly incorporating with porous carbon nanotube buckypaper.* Journal of Reinforced Plastics and Composites, 2015. **35**(2): p. 165-176.
[55] **Wang, X., et al.**, *Tensile strain sensing of buckypaper and buckypaper composites.* Materials & Design, 2015. **88**: p. 414-419.
[56] **Uematsu, Y., T. Kitamura, and R. Ohtani**, *Delamination behavior of a carbon-fiber-reinforced thermoplastic polymer at high temperatures.* Composite Science and Technology, 1995. **53**: p. 333-341.
[57] **Han, S.H., H.J. Oh, and S.S. Kim**, *Evaluation of fiber surface treatment on the interfacial behavior of carbon fiber-reinforced polypropylene composites.* Composites Part B: Engineering, 2014. **60**: p. 98-105.
[58] **Hu, L., D.S. Hecht, and G. Gruner**, *Carbon Nanotube Thin Films Fabrication, Properties, and Applications.* Chemical Reviews, 2009. **110**: p. 5790-5844.
[59] **Wang, S., et al.**, *Carbon Fiber/Carbon Nanotube Buckypaper Interply Hybrid Composites: Manufacturing Process and Tensile Properties.* Advanced Engineering Materials, 2015. **17**(10): p. 1442-1453.

[60] **Lu, S., et al.**, *Real-time cure behaviour monitoring of polymer composites using a highly flexible and sensitive CNT buckypaper sensor*. Composites Science and Technology, 2017. **152**: p. 181-189.
[61] **Li, T., et al.**, *Mechanical enhancement effect of the interlayer hybrid CNT film/carbon fiber/epoxy composite*. Composites Science and Technology, 2018. **166**: p. 176-182.
[62] **Crouch, I.G.**, *Laminated materials and layered structures.* 2017: p. 167-201.
[63] **Qu, B., et al.,** *Enhancement of mechanical properties of buckypapers/polyethylene composites by microwave irradiation.* Composites Science and Technology, 2018. **164**: p. 313-318.
[64] **Park, J.G., et al.**, *Electromagnetic interference shielding properties of carbon nanotube buckypaper composites.* Nanotechnology, 2009. **20**(41): p. 415702.
[65] **Fu, X., et al.**, *Carbon nanotube buckypaper to improve fire retardancy of high-temperature/high-performance polymer composites.* Nanotechnology, 2010. **21**(23): p. 235701.
[66] **Kurt, S.M**., *The UHMWPE Handbook*. 2004, United States of America: Elsevier Academic Press.
[67] **Iannucci, L. and D. Pope**, *High velocity impact and armour design.* Express Polymer Letters, 2011. **5**(3): p. 262-272.
[68] **Figueiredo, A.B.-H.d.S., et al.**, *Response to Ballistic Impact of Alumina-UHMWPE Composites.* Materials Research, 2018. **21**(5).
[69] **Karthikeyan, K., et al.**, *The soft impact response of composite laminate beams.* International Journal of Impact Engineering, 2013. **60**: p. 24-36.
[70] **Sobieraj, M.C. and C.M. Rimnac**, *Ultra high molecular weight polyethylene: mechanics, morphology, and clinical behavior*. J Mech Behav Biomed Mater, 2009. **2**(5): p. 433-43.
[71] **Chunzheng, P.**, *Improved interfacial properties of carbon fiber/UHMWPE composites through surface coating on carbon fiber surface.* Surface and Interface Analysis, 2018. **50**(5): p. 558-563.
[72] **Omnexus**. *Polyethylene (PE) Plastic: Properties, Uses & Application*. Available from: https://omnexus.specialchem.com/selection-guide/polyethylene-plastic.
[73] **Russell, B.P., et al.**, *The high strain rate response of UHMWPE: from fibre to laminate.* 2013. **60**: p. 1-9.
[74] **Ronca, S., et al.**, *Tailoring molecular structure via nanoparticles for solvent free processing of ultra high molecular weight polyethylene composites.* Polymer, 2012. **53**: p. 2897-2907.
[75] **Marissen, R., et al.**, *Multilayered material sheet and process for its preparation*, W.I.P.O.I. Bureau, Editor. 2007.
[76] **Alcock, B. and T. Peijs**, *Polymer Composites-Polyolefin Fractionation-Polymeric Peptidomimetics-Collagens*. 2013: Springer.
[77] **Rastog, S., et al.**, *Unprecedented High-modulus High Strength Tapes and Films of Ultrahigh Molecular Weight Polyethylene via Solvent Free Route.* Macromolecules, 2011. **44**: p. 5558-5568.
[78] **Teijin**, *Endumax® – an ultra-strong thin film with a high modulus*. 2016.
[79] **Atli-Veltin, B**., *Cryogenic Composite Fuel Tanks: The Mechanical Performance of Advanced Composites at Low Temperatures*, in *AIAA/ASCE/AHS/ASC Structures, Structural Dynamics, and Materials Conference*. 2018: Florida.
[80] **Complex, J.P.**, *HDPE for Injection Molding*. Iran.
[81] **Ausman, K.D., et al.**, *Organic Solvent Dispersions of Single Walled Carbon Nanotubes Toward Solutions of Pristine Nanotubes.* The Journal of Physical Chemistry B, 2000. **104**(38): p. 8911-8915.
[82] **Geng, H.-Z., et al.**, *Absorption spectroscopy of surfactant-dispersed carbon nanotube film: Modulation of electronic structures.* Chemical Physics Letters, 2008. **455**(4-6): p. 275-278.

[83] **Angelikopoulos, P. and H. Bock**, *Directed Self Assembly of Surfactants in Carbon Nanotube Materials.* Journal of Physical Chemistry B, 2008. **112B**(44): p. 13793-13801.
[84] **Yang, X., et al.**, *Removal of natural organic matter in water using functionalised carbon nanotube buckypaper.* Carbon, 2013. **59**: p. 160-166.
[85] **Ma, P.-C., et al.**, *Correlation between electrokinetic potential, dispersibility, surface chemistry and energy of carbon nanotubes.* Composites Science and Technology, 2011. **71**(14): p. 1644-1651.
[86] **ASTM**, *Standard Test Method for Short-Beam Strength of Polymer Matrix Composite Materials and Their Laminates*. 2016.
[87] **Adams, D.**, *Thickness-tapered unidirectional composite specimens*, in *Composites World*. 2013.
[88] **Anderson Materials Evaluation**, I. *Differential Scanning Calorimetry (DSC) Thermal Analysis* 2018; Available from: http://www.andersonmaterials.com/dsc.html.
[89] **Intertek**. *Differential Scanning Calorimetry (DSC) Analysis*. Available from: http://www.intertek.com/analysis/dsc/.
[90] **PhotoMetrics**. *Thermogravimetric Analysis (TGA)*. Available from: https://photometrics.net/thermogravimetric-analysis-tga/.
[91] **NanoscienceInstruments**. *Scanning Electron Microscopy*. Available from: https://www.nanoscience.com/techniques/scanning-electron-microscopy/.
[92] **Zhu, F.Y., et al.**, *3D nanostructure reconstruction based on the SEM imaging principle, and applications.* Nanotechnology, 2014. **25**(18): p. 185705.
[93] **Analytical, P. *BET***. Available from: http://particle.dk/methods-analytical-laboratory/surface-area-bet-2/.
[94] **Matshitse, R.**, *Brunauer-Emmett-Teller (BET) surface area analysis*, R. University, Editor.
[95] **Brame, J. and C. Griggs**, *Surface Area Analysis Using the BrunauerEmmett-Teller (BET) Method*, E.R.a.D. Center, Editor. 2016.
[96] **Leddy, N.**, *Surface area and porosity*. 2012, Center for microscopy and analysis.
[97] **Adams, D.** *The short beam shear test*. 2010; Available from: https://www.compositesworld.com/articles/the-short-beam-shear-test.
[98] **Ashrafi, B., et al.**, *Correlation between Young's modulus and impregnation quality of epoxy-impregnated SWCNT buckypaper.* Composites Part A: Applied Science and Manufacturing, 2010. **41**(9): p. 1184-1191.
[99] **Zhang, L., et al.**, *High-density carbon nanotube buckypapers with superior transport and mechanical properties.* Nano Lett, 2012. **12**(9): p. 4848-52.
[100] **Wang, D., et al.**, *Highly oriented carbon nanotube papers made of aligned carbon nanotubes.* Nanotechnology, 2008. **19**(7): p. 075609.
[101] **Kalfon-Cohen, E., et al.**, *Synergetic effects of thin plies and aligned carbon nanotube interlaminar reinforcement in composite laminates.* Composites Science and Technology, 2018. **166**: p. 160-168.
[102] **Lee, J., et al.,** *Advanced carbon fiber composite out-of-autoclave laminate manufacture via nanostructured out-of-oven conductive curing.* Composites Science and Technology, 2018. **166**: p. 150-159.
[103] **Fan, Z., M.H. Santare, and S.G. Advani**, *Interlaminar shear strength of glass fiber reinforced epoxy composites enhanced with multi-walled carbon nanotubes.* Composites Part A: Applied Science and Manufacturing, 2008. **39**(3): p. 540-554.
[104] **Song, Y., et al.**, *Multiscale Laminated Composite Materials*. 2014.

CURRICULUM VITAE

Name Surname **:** Gülşah BAHÇELİ

Place and Date of Birth **:** Bornova - 29.03.1994

E-Mail **:** bahceli@itu.edu.tr

EDUCATION:

M.Sc. : Aeronautics and Astronautics Engineering/ITU

B.Sc. : Aeronautical Engineering/ITU

PROJECTS:

2017 - 2019 : ITU-AYP-2016-17 Project / Project Researcher

2018 - 2019 : ITU-TNO Project/ Researcher

CONFERENCE PROCEEDINGS

"Cryogenic Properties of CNT Reinforced UHMWPE Laminated Composites", Bahçeli, G., Atli-Veltin, B., Wilbers, D., Cebeci, H., AIAA Science and Technology Forum, January 5-11 2019, San Diego, United States of America, oral presentation.